The Prolonged Half-Life of the p53 Missense Variant R248Q Promotes Accumulation and Heterotetramer Formation with Wild-Type p53 to Exert the Dominant-Negative Effect

Nancy Klemm[1], Roman R. Schimmer[1], Nils K. Konrad[1], Flavian Thelen[1], Jonas Fullin[1], Ebru Topçu[1], Christian Koch[1], Milena Treacy[1], Matthew Joseph Leventhal[2,3,4], Marco M. Bühler[5], Veronika Lysenko[1], Alexandre P.A. Theocharides[1], Kari J. Kurppa[6], Stefan Balabanov[1], Tuncay Baubec[7,8], Andrei V. Krivtsov[9,10], Peter G. Miller[11], Scott A. Armstrong[9,10], Benjamin L. Ebert[2,3,4], Markus G. Manz[1], Cesar Nombela-Arrieta[1], and Steffen Boettcher[1]

ABSTRACT

Missense mutants of p53, such as the frequent hotspot variant R248Q, exert a dominant-negative effect (DNE) on wild-type (WT) p53 in cancer cells with monoallelic *TP53* mutations. However, the precise functional and molecular mechanisms of the DNE have remained elusive due to a lack of appropriate model systems. In this study, we developed a variety of model systems, including CRISPR-edited human isogenic cell lines and transcriptional reporter cell lines, and targeted protein degradation assays that were combined with functional and molecular analyses to functionally characterize the DNE. Formation of heterotetramers between R248Q and WT p53 impaired proper WT p53 functionality by preventing DNA binding and subsequent target gene transactivation. Furthermore, the markedly increased protein half-life of R248Q led to supraphysiologic levels of R248Q, which was critically required for the DNE. Drug-induced targeted protein degradation of R248Q to lower the R248Q:WT ratio restored the transcriptional activity of WT p53, induced antiproliferative effects in cancer cells *in vitro*, and elicited strong therapeutic activity *in vivo*. Together, this study provides mechanistic insights into the DNE of p53 missense mutants and indicates that the DNE represents a promising therapeutic target.

Significance: Heterotetramerization between R248Q mutant and wild-type p53 in conjunction with supraphysiologic $p53^{R248Q}$ accumulation underlies the dominant-negative effect, highlighting the need to develop pharmacologic strategies to decrease the elevated R248Q:WT ratio.

See related commentary by Gencel-Augusto and Lozano, p. 1955

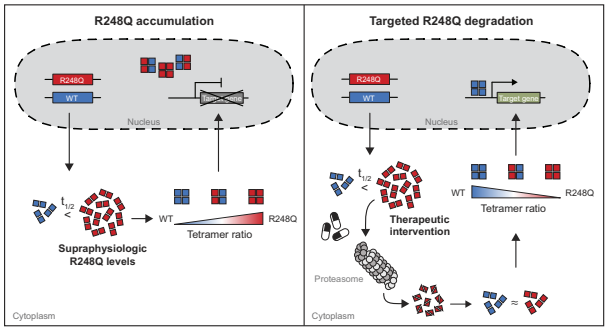

Introduction

Mutations in the tumor-suppressor gene *TP53* are found in about 50% of tumors, making it the most frequently mutated gene in human cancer (1). The unusual mutational spectrum of *TP53*, dominated by missense mutations within p53's central DNA-binding domain, including some hotspot mutations such as $TP53^{R248Q}$, has traditionally been linked to the selection for gain-of-function properties acquired by the resulting aberrant missense mutant p53 variants (2, 3). However, we and others have recently challenged this paradigm, demonstrating that loss-of-function and dominant-negative effects (DNE; refs. 4–8), which are two sides of the same coin, as well as evasion of immunosurveillance (9) shape the mutational landscape of *TP53*.

[1]Department of Medical Oncology and Hematology, University of Zurich and University Hospital Zurich, Zurich, Switzerland. [2]Dana-Farber Cancer Institute, Boston, Massachusetts. [3]The Broad Institute of Massachusetts Institute of Technology and Harvard, Cambridge, Massachusetts. [4]Howard Hughes Medical Institute, Boston, Massachusetts. [5]Department of Pathology and Molecular Pathology, University Hospital Zurich, Zurich, Switzerland. [6]Institute of Biomedicine and Medicity Research Laboratories, University of Turku, Turku, Finland. [7]Department of Molecular Mechanisms of Disease, University of Zurich, Zurich, Switzerland. [8]Genome Biology and Epigenetics, Department of Biology, Institute of Biodynamics and Biocomplexity, Utrecht University, Utrecht, the Netherlands. [9]Department of Pediatric Oncology, Dana-Farber Cancer Institute, Boston, Massachusetts. [10]Division of Hematology/Oncology, Boston Children's Hospital and Harvard Medical School, Boston, Massachusetts. [11]Center for Cancer Research and Center for Regenerative Medicine, Massachusetts General Hospital, Boston, Massachusetts.

Corresponding Author: Steffen Boettcher, Department of Medical Oncology and Hematology, University of Zurich and University Hospital Zurich, Raemistrasse 100, Zurich CH-8091, Switzerland. E-mail: steffen.boettcher@usz.ch

Cancer Res 2025;85:1978–96

doi: 10.1158/0008-5472.CAN-24-1136

Despite its importance, the molecular basis of the DNE has remained elusive. Per definition, the DNE exerted by p53 missense variants leads to a greater degree of p53 pathway inactivation than sole monoallelic loss of p53 expression through, for instance, frame-shift mutations or *TP53* deletions. However, how exactly does monoallelic expression of p53 missense variants impair the function of wild-type (WT) p53 expressed from the remaining WT allele in cells with monoallelic missense mutations? Research into the nature of the DNE has largely been hampered by the lack of appropriate model systems that would allow direct and quantitative comparison of the functional consequences of the various possible allelic configurations of *TP53*. Moreover, experimentally targeting WT and/or mutant p53 protein levels has remained a formidable challenge, but owing to recent technological advances, it has now become feasible. We have therefore set out to combine precise CRISPR/Cas9 genome-editing technology and targeted protein degradation assays with molecular and functional analysis to investigate the molecular mechanism of the DNE. We chose the R248Q variant because it is not only one of the most frequent but also a paradigmatic p53 missense variant, for which we were able to generate novel isogenic model systems allowing us to investigate the DNE exerted by R248Q to an unprecedented degree.

Materials and Methods

General statement on scientific rigor adherence

Given that this work was a preclinical study, scientific rigor adherence categories such as proper reporting of inclusion and exclusion criteria, attrition, sex as a biological variable, subject demographics, blinding methodologies, and performing appropriate power analysis did not apply.

Experiments were replicated at least three times. All parental cell lines were independently authenticated following purchase by performing short tandem repeat profiling and regularly screened for *Mycoplasma* infection using MycoStrip Mycoplasma Detection Kit (rep-mys-50, InvivoGen). Cells were kept in culture for no longer than 3 months prior to thawing of a new batch.

Chemical compounds

Daunorubicin (Dauno; S3035, Selleckchem, RRID: SCR_003823), nutlin-3a (S8059, Selleckchem), lenalidomide (S1029, Selleckchem), pomalidomide (S1567, Selleckchem), iberdomide (S8760, Selleckchem), decitabine (S1200, Selleckchem), and idasanutlin (S7205, Selleckchem) were ordered as lyophilized formulation. Drugs were dissolved in DMSO (D4540, Sigma-Aldrich, RRID: SCR_008988) and stored at −80°C. Aliquoted drugs were freshly thawed and further diluted either in cell culture medium or DMSO to be used in HPD300e Digital Dispenser (HP Inc. Tecan Life Sciences, RRID: SCR_016771).

Acute myeloid leukemia cell lines

Parental human MOLM13 (RRID: CVCL_2119, male) and K563-*TP53* acute myeloid leukemia (AML) cell lines (RRID: CVCL_0004, female) were purchased in 2016 from DSMZ (ACC554) and the ATCC (CCL-243), respectively. Isogenic cell lines were generated by CRISPR-Cas9–mediated genome editing as described previously (6). Cells were cultured in RPMI 1640 (Gibco, Thermo Fisher Scientific, cat. no. 21875091, RRID: SCR_008452) supplemented with 10% heat-inactivated FBS (Gibco, Thermo Fisher Scientific, cat. no. 10500064) and 100 U/mL of penicillin–streptomycin (penicillin–streptomycin 5,000 U/mL, Gibco, Thermo Fisher Scientific, cat. no. 15070063).

All cells were cultured in an incubator of 95% humidity and 5% CO_2 at 37°C and passaged every 2 to 3 days. Cryopreservation of aliquots was done of early passages (P3–P4) and freshly thawed every 2 to 3 months for experiments.

Other cancer cell lines

HCT116 (RRID: CVCL_0291, male) and A549-*TP53* cancer cell lines (RRID: CVCL_0023, male) were purchased in 2020 from the ATCC (CCL-247 and CCL-185, respectively). Isogenic cell lines were generated following the procedure described previously (6). Single-stranded oligonucleotides serving as homology-directed repair templates were designed to perform CRISPR homology-directed repair as described previously (10). Cells were cultured in T25 cell culture flasks, allowed to recover for 7 days, and further expanded. Nonedited cells, i.e., *TP53*^{WT} cells, were depleted by treatment with 5 μmol/L nutlin-3a for 4 days. To this end, 0.5×10^6 cells were seeded in 6-well plates and incubated overnight to allow for cell surface attachment prior to treatment. Assessment of genome-editing efficiency was achieved by ultradeep amplicon next-generation sequencing (NGS) performed at the Massachusetts General Hospital Center for Computational and Integrative Biology DNA core facility (MGH CCIB DNA Core, RRID: SCR_012281). Single-cell cloning was performed by limiting dilution to obtain clones with either loss of *TP53* or R248Q point mutation. Genome-edited clones were first screened by Sanger sequencing (Microsynth), and genotypes were further confirmed by ultradeep amplicon NGS (MGH CCIB DNA Core, RRID: SCR_012281). HCT116 and A549 cells were cultured in Gibco McCoy (modified) Medium 5A (Gibco, Thermo Fisher Scientific, cat. no. 16600082) and Ham's F-12K (Kaighn's) Medium (Gibco, Thermo Fisher Scientific, cat. no. 21127022), respectively, supplemented with 10% FBS, 100 U/mL of penicillin, and 100 μg/mL of streptomycin. All cells were cultured in an incubator of 95% humidity and 5% CO_2 at 37°C. Passaging was performed every 2 to 3 days, and cryopreservation of aliquots was done of early passages (P3–P4) which were freshly thawed every 2 to 3 months.

Lentiviral production and cell transduction

Third-generation lentiviral (LV), replication-defective viruses were generated as previously described (11). In brief, HEK293T cells (RRID: CVCL_0063) were transfected with the LV plasmid encoding the DNA sequence of interest in combination with the packaging plasmid psPAX2 (RRID: Addgene_12260) and envelope plasmid pCAG-VSVG (RRID: Addgene_64084; both kindly provided by Dr. Patrick Salmon, University of Geneva, Geneva, Switzerland). Transfection was performed using JetPRIME transfection reagent (Brunschwig Lab supplies, 114-15) according to the manufacturer's recommendations. Produced LV particles were concentrated with Peg-it (Biozol, SBI-LV825A-1) 2 days after transfection and stored at −80°C until further use.

For cell transduction, 2×10^6 million cells were harvested, resuspended in 8 μg/mL polybrene (Sigma-Aldrich, TR-1003-G) containing cell culture media, and plated in 6-well plates. Virus particles were added to the cells, and spinoculation was performed at 32°C and 800 × *g* for 90 minutes. Media change was performed 24 hours after transduction, and cell lines were further expanded.

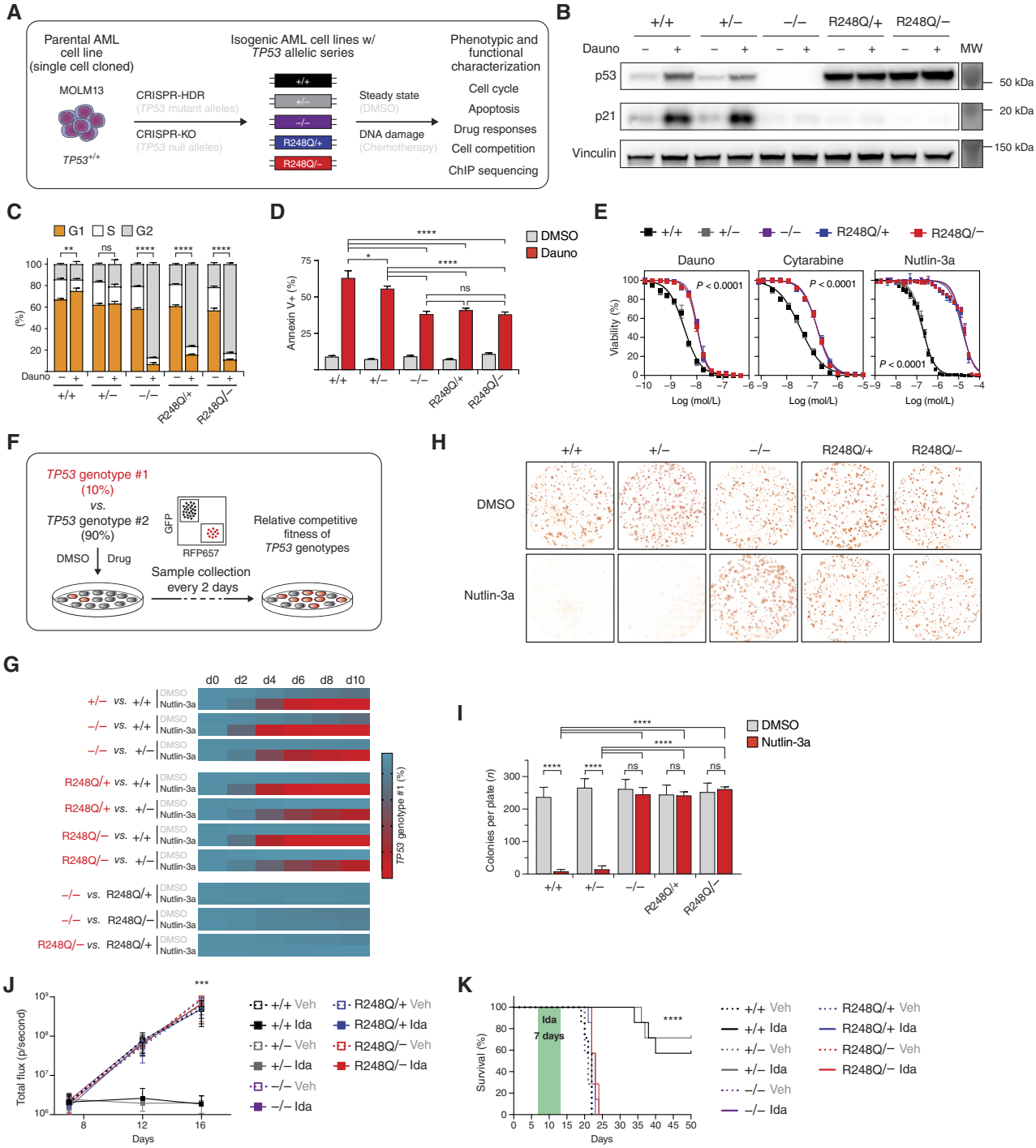

Figure 1.

Characterization of the DNE exerted on WT p53 by the R248Q variant. **A,** Experimental schematic for the CRISPR/Ca9-mediated generation of human isogenic MOLM13-*TP53* AML cell lines and their subsequent phenotypic and functional characterization. CRISPR-HDR, CRISPR-Cas9–mediated homology-directed repair; CRISPR-KO, CRISPR-Cas9–mediated gene knockout. **B,** Whole-cell lysates of isogenic MOLM13-*TP53* AML cell lines of the indicated genotypes treated for 3 hours with either DMSO or 100 nmol/L Dauno were separated on a polyacrylamide gel and immunoblotted for p53, p21, and vinculin (representative blot of $n = 3$ independent experiments). **C,** Cell-cycle distribution of isogenic MOLM13-*TP53* isogenic AML cell lines of the indicated genotypes treated for 6 hours with either DMSO or 100 nmol/L Dauno as determined by CytoPhase Violet staining ($n = 3$ independent experiments). Bar graphs represent averages. Error bars, SEM. **, $P \leq 0.01$; ****, $P \leq 0.0001$, one-way ANOVA, Tukey multiple comparison. **D,** Fraction of apoptotic MOLM13-*TP53* isogenic AML cell lines as determined by Annexin V staining after treatment with either DMSO or 100 nmol/L Dauno for 72 hours ($n = 3$ independent experiments). Bar graphs represent averages. Error bars, SEM. *, $P \leq 0.05$; ****, $P \leq 0.0001$, two-way ANOVA, Tukey multiple comparison. **E,** Cell viability of MOLM13-*TP53* (*Continued on the following page.*)

Cancer cell lines expressing oligomerization-deficient R248Q variants

Site-directed mutagenesis was performed to introduce R248Q point mutation in *TP53* encoded by pcDNA flag p53 (gift from Thomas Roberts, Addgene plasmid #10838, http://n2t.net/addgene:10838; RRID: Addgene_10838) as well as additional mutations inhibiting the oligomerization capability of WT and R248Q protein variants (i.e., L344A: introducing tetramerization deficiency; L344P: introducing dimerization deficiency; an ΔOD: deletion of the oligomerization domain (OD), introducing dimerization deficiency). Mutagenesis primers were designed using NEBaseChanger (New England Biolabs, version 1.3.3, RRID: SCR_013517), and site-directed mutagenesis was performed using Q5 Site-Directed Mutagenesis Kit (New England Biolabs, #E0554) according to the manufacturer's recommendations. Afterward, mutagenized p53 variants were amplified and cloned into Cilantro 2 (a great gift from Benjamin Ebert, Addgene plasmid #74450, http://n2t.net/addgene:74450, q RRID: Addgene_74450) while cutting out the included enhanced green fluorescent protein (EGFP) sequence.

Cancer cell lines expressing degradable R248Q(-GFP) or degradable GFP/BFP

Isogenic K562-*TP53*^{WT} or MOLM-*TP53*$^{+/-}$ cells expressing either degradable R248Q(-GFP) or degradable GFP/blue fluorescent protein (BFP) and mCherry were established by PCR amplification of ZFP91-IKFZ3 super-degron sequence (5′-TTG CAG TGC GAA ATA TGC GGC TTT ACC TGC CGC CAG AAA GGT AAC CTC CTC CGC CAC ATT AAA CTG CAC-3′, short: super-degron; ref. 12). Amplification products were cloned into pcDNA flag p53 (gift from Thomas Roberts, Addgene plasmid #10838, http://n2t.net/addgene:10838; RRID: Addgene_10838) to N-terminally tag p53 with the super-degron sequence. Afterward, site-directed mutagenesis was performed to introduce R248Q point mutation in p53 (p53^{R248Q}). Mutagenesis primers were designed using NEBaseChanger (New England Biolabs, version 1.3.3), and site-directed mutagenesis was performed using Q5 Site-Directed Mutagenesis Kit (New England Biolabs, #E0554) according to the manufacturer's recommendations. Finally, N-terminally super-degron tagged R248Q (or GFP/BFP) was amplified and cloned into Cilantro 2 (a gift from Benjamin Ebert, Addgene plasmid #74450, http://n2t.net/addgene:74450, q RRID: Addgene_74450) to obtain a LV expression plasmid encoding (C-terminally GFP-tagged) degron-R248Q (or degron-GFP/BFP) and mCherry as reference fluorochrome via an internal ribosomal entry site (IRES). Lentivirus production and transduction was performed as described above. Prior to performing experiments, cells were sorted to select for mCherry and GFP or BFP double-positive cells. Freshly sorted cells were used for further experiments for up to 2 to 3 months.

Western blot analysis

Cells were washed in PBS and lysed in Pierce RIPA lysis buffer (Thermo Fisher Scientific, Cat. No. 89900) freshly supplemented with cOmplete ULTRA Tablets (Mini, EDTA-free, EASYpack Protease Inhibitor Cocktail, 5892791001 Sigma-Aldrich). Equal protein amounts, as quantified by Pierce BCA Protein Assay Kit (Thermo Fisher Scientific, cat. no. 23225,), were loaded and ran on NuPAGE 4% to 12% Bis-Tris Midi gels (Invitrogen, WG1403BOX, 1.0 mm) or Bolt Bis-Tris Plus 4% to 12% Mini gels (Invitrogen, NW04125BOX, 1.0 mm, WedgeWell format). Proteins were transferred to Amersham Hybond P polyvinylidene difluoride (PVDF) Western blotting membranes (Merck, RRID: SCR_001287, GE10600023) and blotted for p53 (mouse mAb DO-1, Cell Signaling Technology, RRID: SCR_002071, #18032, RRID: AB_2798793), p21 (rabbit mAb 12D1, Cell Signaling Technology, #2947, RRID: AB_823586), GFP (rabbit polyclonal antibody, Abcam, ab290, RRID: AB_303395), and vinculin (rabbit mAb, EPR8185, ab129002, RRID: AB_11144129). Goat anti-mouse horseradish peroxidase (HRP; Genesee Scientific, 20-304), goat anti-rabbit HRP (Genesee Scientific, #20-303), and Immobilon Forte Western HRP substrate (Merck, Millipore, RRID: SCR_008983, WBLUF) were used to visualize the blot using Fusion Solo S Western blot imager (Vilber, RRID: SCR_023580).

Western blot quantification

Protein quantification after Western blotting was performed using ImageJ (ImageJ, RRID: SCR_003070, version 1.54f, NIH). The same selection area was used to select individual protein bands, and the gray mean value was measured. Similarly, the mean gray value of the membrane background was measured and subtracted uniformly across all measured bands. If applicable, the intensity of each measured protein band was normalized to the background corrected values of the loading control.

Cell-cycle analysis

1×10^6 human MOLM13-*TP53* isogenic AML cell lines (+/+, +/−, −/−, R248Q/+, and R248Q/−) and 4×10^6 MOLM13-*TP53*$^{+/-}$ cells expressing either degradable GFP (degGFP) or degradable R248Q (degR248Q) were seeded in 12-well plates and T25 flasks, respectively. MOLM13-*TP53* isogenic AML cells were treated with DMSO or 100 nmol/L Dauno, whereas MOLM13-

(*Continued*.) isogenic AML cell lines was determined using the CellTiter-Glo reagent after being exposed to increasing concentrations of the indicated drugs for 72 hours ($n = 3$ independent experiments). Symbols represent averages. Error bars, SD, Friedman test. **F,** Schematic depicting the experiment principle of the *in vitro* competition assay. Fluorescently labeled MOLM13-*TP53* isogenic AML cell lines of various *TP53* genotypes were cocultured at a 1:9 ratio in the presence of DMSO or 1 μmol/L nutlin-3a, and the relative fractions of each genotype were determined by flow cytometry every other day for 10 days. **G,** Heatmaps depict the results of the *in vitro* competition assays described in **F**. $n = 3$ independent experiments; color-coded averages are shown. d, day. **H,** Representative images of a colony-forming unit assay. MOLM13-*TP53* isogenic AML cell lines of the indicated genotypes were cultured for 7 days in methylcellulose-based medium with DMSO or 2.5 μmol/L nutlin-3a. Images were taken using a Leica DMI6000B inverted microscope, and analysis was performed using the Colony Area ImageJ plugin, followed by manual counting of the colonies (representative images of $n = 3$ independent experiments). **I,** Counted colonies from colony-forming unit assay as described in **H**. $n = 3$ independent experiments. Bar graphs represent averages. Error bars, SEM. ****, $P \le 0.0001$, one-way ANOVA, Tukey multiple comparison. **J,** Quantification of the bioluminescent signal (i.e., total flux per second) for each group of mice 12 and 16 days after sublethal irradiation and subsequent injection with MOLM13-*TP53*-GFP-luciferase isogenic AML cell lines (of the indicated genotypes). One week after injection, mice were treated with idasanutlin (Ida, 25 mg/kg of BW per day) or vehicle (Veh) for seven consecutive days. $n = 7$ animals per group. Symbols represent averages. Error bars, SD; ***, $P \le 0.001$, Mann–Whitney test. **K,** Survival analysis of NSG mice engrafted with MOLM13-*TP53*-GFP-luciferase isogenic AML cell lines of the indicated genotypes and treated with idasanutlin (25 mg/kg of BW per day) or vehicle for seven consecutive days. $n = 7$ animals per group. ****, $P \le 0.0001$, Kaplan–Meier simple survival analysis. ns, nonsignificant.

TP53$^{+/-}$-degGFP and -degR248Q cells were treated with either DMSO, 2.5 μmol/L nutlin-3a, and/or 1 μmol/L Iberdomide for 24 hours at 37°C. Following treatment, no more than 1×10^5 cells of each treatment condition were collected in 96-well plates, resuspended in CytoPhase Violet (BioLegend, RRID: SCR_001134, cat. no. 425701) staining master mix as advised by the manufacturer's protocol, and incubated for 90 minutes at 37°C. Analysis of cell-cycle distribution was performed by flow cytometry using a BD LSRFortessa flow cytometer (BD Biosciences, RRID: SCR_013311), and acquired data were analyzed via FlowJo software (v10.0.7, FlowJo, LCC).

Apoptosis assay

Isogenic MOLM13-*TP53* AML cells (+/+, +/−, −/−, R248Q/+, and R248Q/−) and MOLM13-*TP53*$^{+/-}$-degGFP and -degR248Q cells were seeded at a density of 1×10^6 cells per well in 12-well plates and 4×10^6 cells per T25 flask, respectively. Whereas MOLM13-*TP53* AML cells were treated with DMSO or 100 nmol/L Dauno, MOLM13-*TP53*$^{+/-}$-degGFP and -degR248Q cells were treated with either DMSO, 2.5 μmol/L nutlin-3a, and 1 μmol/L iberdomide or a combination of the latter two drugs for 24 to 72 hours. Cell samples were collected every 24 hours, and apoptosis was determined by staining for phosphatidylserine via Annexin V allophycocyanin staining according to the manufacturer's protocol (BioLegend, cat. no. 640920) in combination with 4′,6-15 diamidino-2-phenylindole dilactate (DAPI; Invitrogen, cat. no. D1306). Flow cytometric analysis was performed using the BD LSRFortessa flow cytometer (BD Biosciences, RRID: SCR_013311). Data were analyzed using FlowJo software (v10.0.7, FlowJo, RRID: SCR_008520, FlowJo, LLC).

Drug sensitivity assay

MOLM13-*TP53* isogenic AML cells were seeded in opaque-walled 96-well flat-bottom culture plates yielding a cell concentration of 1×10^4 cells per well and incubated with increasing concentrations of Dauno, nutlin-3a, and decitabine. Limiting dilutions of the used drugs were achieved using HPD300e Digital Dispenser (HP Inc., Tecan Life Sciences, RRID: SCR_016771). Plates were sealed with Nunc sealing tape (white Rayon, breathable, sterile, 241205, Thermo Fisher Scientific) to prevent excessive evaporation. Following 72 hours of treatment, cell viability was assessed using the CellTiter-Glo luminescent assay (G7572, Promega, RRID: SCR_006724). The luminescent signal was acquired using the Biotek Synergy LX (SLXFTS) luminometer (Agilent Technologies, RRID: SCR_013575). To generate dose–response curves, cell viabilities were normalized to vehicle-treated controls and fit using nonlinear regression analyses via GraphPad Prism software (version 10.2.1, RRID: SCR_002798).

Competitive cell growth assay

Isogenic MOLM13-*TP53* AML cells (expressing RFP657) of various genotypes were seeded at a concentration of 0.96×10^4 cells per well in a 96-well flat-bottom plate in a 9:1 ratio with MOLM13-*TP53* cells of other MOLM13-*TP53* AML cells of various genotypes (expressing GFP) at a concentration of 0.04×10^4 cells per well. The cell line that was expected to gain a survival advantage over time was seeded at the lower concentration, as detailed in the "Results" section. Seeded competitions were cocultured in the presence of 1 μmol/L nutlin-3a or DMSO for up to 10 days. Similarly, K562-*TP53*^{WT}-deg.R248Q cells were cocultured with isogenic K562-*TP53*^{WT} cells in a ratio of 1:9 or with isogenic K562-*TP53*^{R248Q} cells in a ratio of 9:1, reaching a total cell concentration of 10,000 cells per well in a 96-well flat-bottom plate. Likewise, MOLM13-*TP53*$^{+/-}$-degR248Q cells were seeded in a ratio of 9:1 with isogenic MOLM13-*TP53*$^{R248Q/-}$ or with MOLM13-*TP53*$^{+/-}$ in inversed ratio aiming for the same cell concentration per well. Generally, the experimental setup was in accordance with the above-mentioned strategy to seed the cell line with the suspected competitive advantage over time at the lower cell density. Competitions including cells expressing degGFP or degR248Q were cocultured with DMSO, 2.5 μmol/L nutlin-3a, and/or 1 μmol/L iberdomide for 8 days.

Every 2 days, a cell sample was taken for flow cytometric analysis via the BD LSRFortessa flow cytometer (BD Biosciences, RRID: SCR_013311) using a high-throughput sampler (Becton Dickinson). To maintain the nutlin-3a and/or iberdomide concentration over time, wells were replenished with fresh medium and the appropriate concentration of nutlin-3a and/or iberdomide after each measurement.

Colony formation assay

To assess the clonogenic potential of the isogenic MOLM13-*TP53* AML cells as well as MOLM13-*TP53*$^{+/-}$-degGFP and -degR248Q cells, a colony formation assay was performed for which first 3,000 cells were diluted in 200 μL of FBS per treatment group. The first-mentioned cell lines were treated with DMSO or 2.5 μmol/L nutlin-3a, whereas the latter were treated with either DMSO, 2.5 μmol/L nutlin-3a, and/or 1 μmol/L iberdomide. Therefore, appropriate drugs were added to the prediluted cell suspension in 10× concentration, mixed by vortexing, and added to 1 mL of MethoCult H4230 (STEMCELL Technologies, RRID: SCR_013642, cat. no. #04330). After allowing the solution to sit for 5 minutes, the cell suspension was transferred to 6-well cell culture dishes and incubated at 37°C in a humidified chamber for 7 days.

Image acquisition was performed using an inverted microscope (Leica DMI6000B, RRID: SCR_018713, Leica microsystems), and image analysis was performed via ImageJ (RRID: SCR_003070, version 1.54f, NIH) software. The images were processed via the Colony Area ImageJ plugin, and formed colonies were counted manually.

Animal experiments

The housing and experimental procedures of all animals were approved by the Cantonal Veterinary Office (Zurich, Switzerland) under the license number 35715 and following the Animal Research: Reporting of *In Vivo* Experiments guidelines. All animal experiments were conducted in 8- to 12-week-old female immunodeficient NOD/SCID/IL2Rγ-null (NSG) mice (purchased from Charles River Laboratories, RRID: SCR_003792). Animal maintenance was performed under specific pathogen-free conditions at the Laboratory Animal Services Center, and animals were allowed to acclimatize for 1 week prior to the start of the experiments. The AML xenograft models were established by intravenous injection of either 0.1×10^6 luciferase–GFP-expressing MOLM13-*TP53* cells (either +/+, +/−, −/−, R248Q/+, or R248Q/−) or luciferase–GFP-expressing MOLM13-*TP53* cells carrying a WT allele and expressing either tetramerization-proficient (R248Q) or tetramerization-deficient (R248Q-L344P) R248Q variants or 0.08×10^6 luciferase–GFP-expressing MOLM13-*TP53*$^{+/-}$ cells with degR248Q or BFP into sublethally irradiated (100cGy) NSG mice. After 5 to 7 days, animals were further allocated to receive treatment.

To assess the leukemic burden caused by isogenic MOLM13-*TP53* cells and MOLM13-*TP53* cells carrying a WT allele

and expressing either tetramerization-proficient (R248Q) or tetramerization-deficient (R248Q-L344P) R248Q variants, animals received either 25 mg/kg body weight (BW)/d idasanutlin or vehicle (40% PEG300, 5% Tween80, 50% ddH20, and 10% DMSO) via oral gavage 7 days after injection for 7 days. For xenograft experiments using MOLM13-*TP53*$^{+/-}$ cells with degR248Q or BFP, animals received either 10 mg/kgBW twice a day iberdomide or vehicle via oral gavage 5 days after injection for 10 days and/or 25mg/kgBW/d idasanutlin or vehicle via oral gavage starting 7 days after injection for 7 days.

Following 12 and 16 days after injection, tumor burden was assessed by bioluminescent imaging. Therefore, mice were anaesthetized and received 150 mg/kg BW D-luciferin (Xenolight D-Luciferin K+ salt bioluminescent substrate, cat. no. 122799, PerkinElmer, Inc.) intraperitoneally. Xenogen IVIS 200 machine (PerkinElmer IVIS Spectrum *In Vivo* Imaging System, RRID: SCR_018621) with the Living Image Software (Caliper Life Sciences, RRID: SCR_025130) was used for image acquisition. The following criteria indicated whether mice were considered to have reached the endpoint: paralysis of any leg, moribund appearance (i.e., unresponsive to stimuli, labored respiration, and limited ambulation), and BW loss of more than 15% to 20% of starting weight or dehydration unresponsive to NaCl injections. With the fulfillment of any of the aforementioned criteria, mice were sacrificed, and the day of death was noted as the day of sacrifice for survival analysis. For all xenograft experiments mentioned above, seven mice were used per group.

Immunofluorescence analysis

A total of 2×10^6 isogenic MOLM13-*TP53* cells were seeded in 6-well plates, treated with 100 nmol/L Dauno or DMSO for 3 hours at 37°C, and subsequently washed with PBS prior to incubation with CellBrite Fix 640 membrane stain (Biotium Inc., RRID: SCR_013538, #30089) for 30 minutes at room temperature according to the manufacturer's protocol. Afterward, cells were seeded and allowed to settle for 30 minutes at 37°C on precleaned micro slides (Corning, 2948-75X25) treated with 0.01% poly-L-lysine (0.01%, sterile-filtered, BioReagent, Merck, P4707) wells were generated using a PAP pen (Abcam, RRID: SCR_012931, ab2601). Cells were fixed with with 4% paraformaldehyde (16% w/v aqueous solution, methanol-free, Alfa Aesar, 43368) for 10 minutes at room temperature and subsequently permeabilized with 0.02% Triton X-100 (Merck, 9036-19-5) in PBS for 5 minutes at room temperature. Blocking solution (0.02% Triton-X-100 in PBS with 10% goat serum-Abcam, ab7481) was applied for 1 hour prior to the addition of primary antibody targeting p53 (mouse mAb DO-1, RRID: AB_2798793, Cell Signaling Technology, #18032), which was incubated overnight at 4°C in a humidified chamber. Lastly, cells were stained with secondary Alexa Fluor 488 goat anti-mouse IgG (H + L) antibody (cross-adsorbed secondary antibody, Invitrogen, Thermo Fisher Scientific, cat. no. A-11001) for 1 hour at room temperature and mounted with 4′,6-15 diamidino-2-phenylindole dilactate–containing mounting media (Aqueous, Fluoroshield, Abcam, ab1041394) using cover glasses (Menzel GmbH + Co KG, 2726C). Antibody solutions were prepared in blocking buffer at all times. Immunodetection of antibody-stained proteins was performed using a confocal microscope (Leica DMI6000B, Model SP8, Leica Microsystems, RRID: SCR_018169). ImageJ (version 1.54f, NIH) software was used to analyze the recorded images. A global threshold was set for all the images to exclude background signal.

Chromatin immunoprecipitation

Chromatin immunoprecipitation (ChIP) was performed as previously described (6). Briefly, crosslinking of cells was performed with 1% methanol-free formaldehyde (Thermo Fisher Scientific, #28906), whereas stripping of cytoplasm was achieved by treatment with 50 mmol/L Tris-HCl. Following nuclei precipitation via centrifugation, nuclei were resuspended in 66 mmol/L Tris-HCl and sheared using an E220 sonicator (Covaris, RRID: SCR_019817). IP was performed using anti-p53 antibodies (DO-1, Abcam, #1101, RRID: AB_297667) and Protein G Dynabeads (Thermo Fisher Scientific, #10003D). Reverse-crosslinkage of immunoprecipitated DNA was performed, and quantification was achieved by ScreenTape HS D1000 (Agilent) and Qubit (Thermo Fisher Scientific, RRID: SCR_018095). llumina-compatible sequencing libraries were prepared using SMARTer ThruPLEX DNA-Seq Kit (Takara Bio Inc., RRID: SCR_021372, #R400675). Finally, to obtain paired-end reads, sequencing was performed on a NextSeq 550 Sequencing System (RRID: SCR_016384, Illumina, RRID: SCR_010233). Data for isogenic MOLM13-*TP53* cells with +/+, −/−, and R248Q/− alleles were published previously (6) and repurposed in the current study to compare to the results of MOLM13-*TP53* cells with R248Q/+ alleles, which were generated in parallel but not previously published.

RT-qPCR

A total of 2×10^6 isogenic MOLM13-*TP53* cells were harvested and seeded in 6-well plates and treated with 100 nmol/L Dauno or DMSO for 6 hours at 37°C. Afterward, cells were washed in PBS, and RNA isolation was performed using RNeasy Kit (Qiagen, RRID: SCR_008539, #74106). Isolated total RNA was used to perform cDNA synthesis using High-Capacity cDNA Reverse Transcription Kit (Applied Biosystems, RRID: SCR_005039, 4368814). Synthesized cDNA was analyzed by RT-qPCR using TaqMan Gene Expression Master Mix (Thermo Fisher Scientific, #4369016) and TaqMan Gene Expression Assays (*CDKN1A*, Hs00355782_m1; *MDM2*, Hs00540450_s1; *ACTB*, Hs99999903_m1) in 348-well plates. The PCR reaction was performed on a 7900HT Fast-Real-Time PCR System (Applied Biosystems).

Glutaraldehyde fixation

Following treatment of 2.5×10^6 cells with 100 nmol/L Daunor or DMSO for 3 hours at 37°C, cells were collected, washed in PBS, and lysed in IGEPAL lysis buffer (50 mmol/L Trizma Hydrochlorid (Merck, T5941), pH8, 150 mmol/L NaCl (Merck, S7653), 1 mmol/L EDTA (Sigma-Aldrich, ED), and 1% IGEPAL CA-630 (Sigma-Aldrich, I8896) supplemented with cOmplete ULTRA Tablets (Mini, EDTA-free, EASYpack Protease Inhibitor Cocktail, 5892791001 Sigma-Aldrich). Cell lysates were treated with 0.03% glutaraldehyde (Carl Roth, 4157.2) for 20 minutes at room temperature, fixation was terminated by addition of 4X Bolt LDS Sample Buffer (Thermo Fisher Scientific, B0007) and 10X Bolt Sample Reducing Agent (Thermo Fisher Scientific, B0009), and subsequent incubation was carried out at 95°C for 5 minutes prior to application to Western blot analysis. Western blotting was performed as described above, and the PVDF membrane was blotted for p53 (mouse mAb DO-1, RRID: AB_2798793, Cell Signaling Technology, #18032).

Foerster-resonance electron transfer assay

The donor fluorochrome ECFP, and nonabsorbent, nonfluorescent control acceptor fluorochrome Amber were amplified from

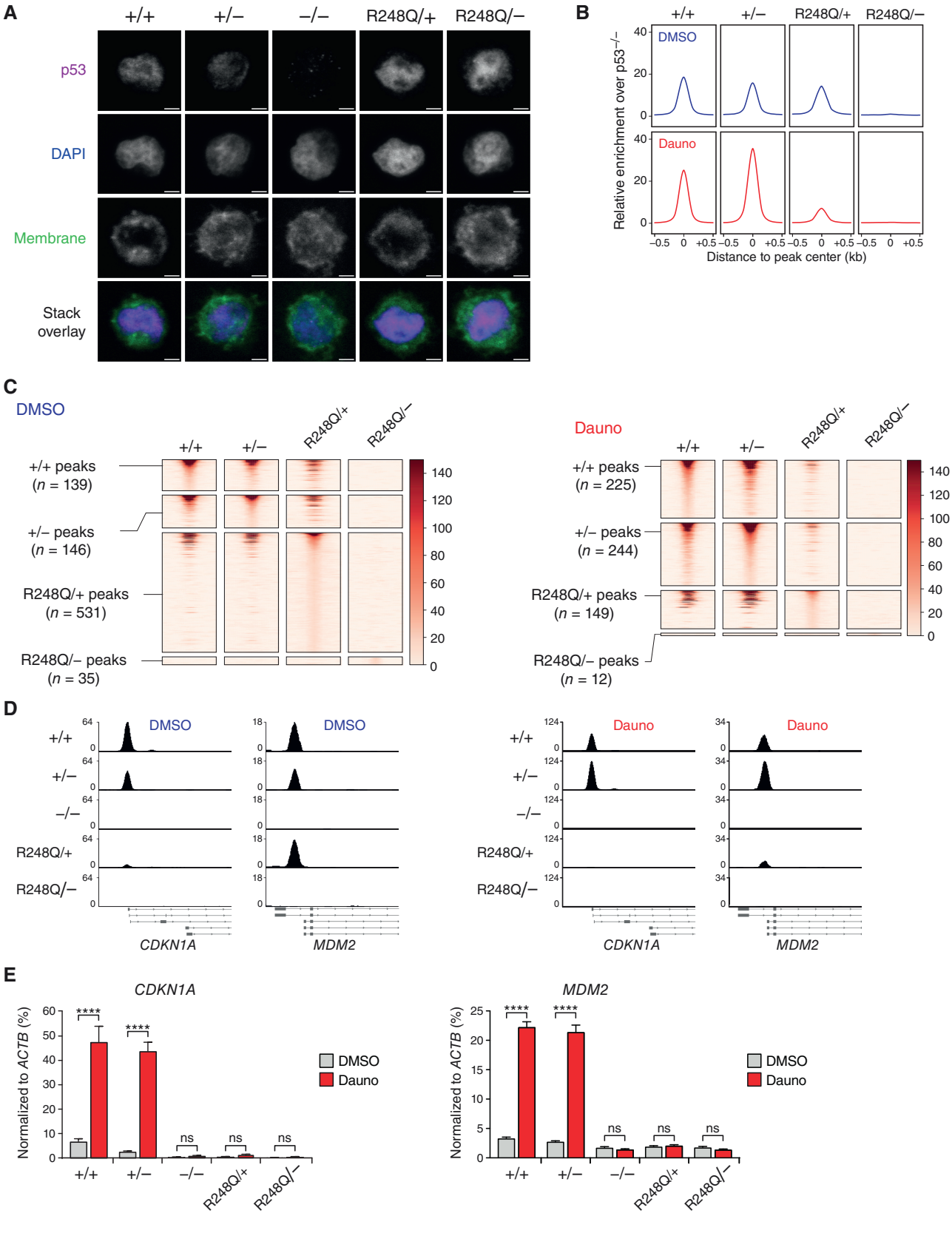

pAquaN1 (gift from Fabienne Merola, Addgene plasmid #42888, http://n2t.net/addgene:42888, RRID: Addgene_42888) and Amber N1 (gift from Steven Vogel, Addgene plasmid #27798, http://n2t.net/addgene:27798, RRID: Addgene_27798), respectively, and N-terminally tagged to a glycine-rich flexible linker [5′- 4×-(GGC) TCC 3×-(GGC) GGA TCC-3′]. Furthermore, site-directed mutagenesis was performed to introduce C67Y in Amber (AMBER, RRID: SCR_016151) to convert the nonfluorescent protein to the acceptor fluorchrome mVenus. Subsequently, mVenus was N-terminally tagged to the glycine-rich linker as stated above. Finally, linker-tagged ECFP, Amber, and mVenus were amplified and cloned into Flag-p53/pRK5 (gift from Xiaolu Yang, Addgene plasmid #39237, http://n2t.net/addgene:39237; RRID: Addgene_39237) previously modified to express the p53^{WT} or p53^{R248Q} variant in in combination with oligomerization-deficient variants (L344A, L344P, and ΔOD). The resulting plasmids carried C-terminally ECFP, Amber, or mVenus tagged p53 variants applicable for transient overexpression of those variants and analysis of protein–protein interactions via Foerster-resonance electron transfer (FRET).

To perform FACS-FRET, 0.5 × 10^6 K562-*TP53*^{null} cells were harvested, spun down, and resuspended in 50 μL PBS, whereas plasmids of interest were mixed in equimolar ratios in 50ul of Nucleofector solution V solution (Lonza, RRID: SCR_000377) to obtain a total plasmid concentration of 5 μL per electroporation reaction. The cell suspension and plasmids were mixed in a ratio of 1:1, yielding in a final volume of 100 μL. Electroporation was carried out using the Nucleofector 2b System (Lonza, RRID: SCR_022262) following the cell line–specific recommendations of the manufacturer's protocol. Electroporated cells were transferred to 12-well plates equipped with preconditioned cell culture media and allowed to recover for 12 hours.

Following, cells were treated with 2.5 μmol/L nutlin-3a for 24 hours prior to flow cytometric analysis using BD LSRFortessa (BD Biosciences, RRID: SCR_013311). FACS-FRET measurement was performed using 405- and 488-nm lasers. To measure ECFP as well as FRET, cells were excited using a 405-nm laser, whereas fluorescence was collected for ECFP using the 450/50 filter and for FRET-signal using the 525/50 filter. mVenus-positive cells were detected by using the 488-nm laser, whereas fluorescence signal was collected using the 530/30 filter.

Transient expression vectors

Transient p53 expression plasmids to express either WT p53 or R248Q in combination with oligomerization-deficient variants (L344A, L344P, and ΔOD) were obtained by site-directed mutagenesis of Flag-p53/pRK5 (gift from Xiaolu Yang, Addgene plasmid #39237, http://n2t.net/addgene:39237; RRID: Addgene_39237). The NEBaseChanger (New England Biolabs, version 1.3.3) was used as tool to design mutagenesis primers, and mutagenesis was performed using Q5 Site-Directed Mutagenesis Kit (New England Biolabs, #E0554) according to the manufacturer's recommendations.

Transient p53 expression via electroporation

K562-*TP53*^{WT}-p21-GFP reporter cells were generated using the endogenous fluorescent tagging technique as described previously (13) and further CRISPR-engineered to express *TP53*^{null} or *TP53*^{R248Q} alleles. 0.5 × 10^6 K562-*TP53*^{null}-p21-GFP (reporter cells) were harvested, spun down, and resuspended in 50 μL PBS, whereas plasmids of interest were mixed in in 50 μL of Nucleofector solution V (Lonza, VCA-1003) to obtain a concentration of 5 μg per electroporation reaction. The cell suspension and plasmids were mixed in a ratio of 1:1, yielding in a final volume of 100 μL. Electroporation was carried out using the Nucleofector 2b System (Lonza) following the cell line–specific recommendations of the manufacturer's protocol. Electroporated cells were transferred to 12-well plates loaded with preconditioned cell culture media and allowed to recover for 12 hours. Cells were treated with 2.5 μmol/L nutlin-3a or DMSO for 24 hours prior to flow cytometric analysis using the BD LSRFortessa flow cytometer (BD Biosciences, RRID: SCR_013311).

Hematoxylin and eosin and p53 IHC staining

Representative cases of hematologic malignancies with *TP53*^{WT} or *TP53*^{R248Q} were retrieved from the archives of the Department of Pathology and Molecular Pathology of the University Hospital Zurich, with appropriate written informed patient consent. The study was conducted in accordance with the Declaration of Helsinki and was approved by the Cantonal Ethics Commission of Zurich (BASEC 2018-01618). p53 IHC was performed with a mouse anti-human mAb (clone DO-7, Agilent, cat. #GA616, RRID: AB_2889978) on an automated Ventana Benchmark ULTRA system (Roche Diagnostics, RRID: SCR_025506).

cDNA sequencing

A total of 2 × 10^6 million cells were harvested and washed in PBS, and RNA isolation was performed using RNeasy Kit (Qiagen, #74106). High-Capacity cDNA Reverse Transcription Kit (Applied Biosystems, 4368814) was used for reverse transcription. Synthesized cDNA was amplified spanning the missense mutant containing region of interest. Amplified cDNA was purified and sequenced at the MGH CCIB DNA Core (RRID: SCR_012281).

Figure 2.

R248Q impairs the ability of WT p53 to bind to promoter DNA and to transactivate expression of target genes. **A,** Immunofluorescence microscopy images showing p53 (magenta), DAPI (blue), and CellBrite Fix 640 membrane stain (green) in MOLM13-*TP53* isogenic AML cell lines treated for 3 hours with 100 nM Dauno ($n = 3$ independent experiments; one representative example is shown; confocal microscope Leica DMI6000B, 63× objective). Scale bar, 2.5 μm. **B,** ChIP followed by NGS in isogenic MOLM-*TP53* AML cell lines of the indicated genotypes after treatment with DMSO or 100 nmol/L Dauno for 6 hours. Plots show genome-wide relative enrichment of p53 variants (WT or R248Q) over p53^{null} cells over TSS-proximal regions (−10 kb to first intron). **C,** Tornado plots of WT and R248Q ChIP-seq peaks over TSS-proximal regions (−10kb, first intron with a horizontal window of 1 kb around the peak center) in isogenic MOLM-*TP53* AML cell lines of the indicated genotypes. Cells were treated as described in **B**. Plots show relative enrichment and mutual overlap of the peaks identified in each cell line. **D,** Representative Integrative Genome Viewer images depicting the ChIP-seq peaks for p53 over the TSS of *CDKN1A* or *MDM2* in isogenic MOLM-*TP53* AML cell lines of the indicated genotypes after treatment as described in **B**. **E,** Relative expression of *CDKN1A* and *MDM2* transcripts normalized to *ACTB* in isogenic MOLM-*TP53* AML cell lines of the indicated genotypes after treatment with DMSO or 100 nmol/L Dauno for 6 hours ($n = 3$ independent experiments). Bar graphs represent averages. Error bars, SD. ns, nonsignificant; ****, $P \leq 0.0001$, one-way ANOVA, Tukey multiple comparison.

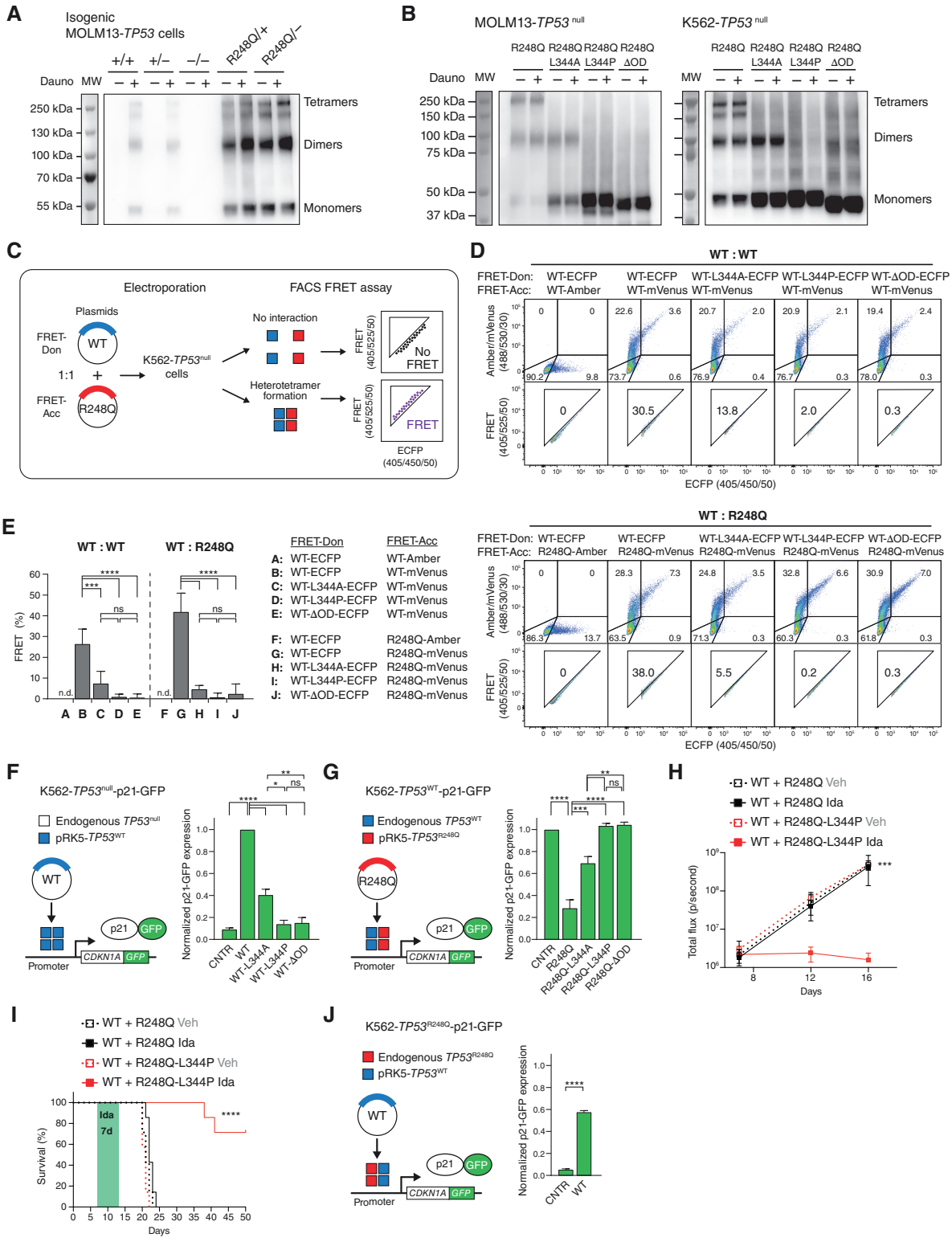

Figure 3.

Heterotetramers consisting of R248Q and WT p53 are transcriptionally inactive, but overexpression of WT p53 can overcome the DNE of R248Q. **A,** MOLM13-*TP53* isogenic cell lines were treated with DMSO or 100 nmol/L Dauno for 3 hours, followed by collection of whole-cell protein lysates by using IGEPAL lysis buffer. Lysates were fixed with 0.03% glutaraldehyde and subsequently separated on a polyacrylamide gel under nonreducing conditions. The PVDF membrane was immunoblotted for p53 ($n = 3$ independent experiments; one representative blot is shown). **B,** MOLM13-*TP53*^{null} or (*Continued on the following page.*)

Protein half-life

A total of 3×10^6 untreated cells were seeded in 12-well plates and incubated at 37°C, and 1 mg/mL cycloheximide (Merck, 01810) was added at varying time points every 30 to 5 minutes. Following a maximum treatment time of 3 hours, cells were harvested, washed with PBS, and lysed in Pierce RIPA lysis buffer (Thermo Fisher Scientific, cat. no. 89900). Subsequently, samples were applied to Western blot analysis as described above, and the PVDF membrane was blotted for p53 (mouse mAb DO-1, RRID: AB_2798793, Cell Signaling Technology, #18032).

Statistical analysis

Statistical significance testing was determined using GraphPad Prism by the indicated tests (GraphPad Prism, RRID: SCR_002798, version 10.2.1).

Data availability

The cDNA sequencing data generated in this study are publicly available in the Sequence Read Archive at PRJNA1198040. The ChIP sequencing data have been deposited in Gene Expression Omnibus at GSE284299. All other raw data generated in this study are available upon request from the corresponding author.

Results

The p53 missense variant R248Q exerts a DNE on WT p53

To unravel the DNE exerted by the p53 missense variant R248Q, we utilized CRISPR genome-edited human MOLM13-*TP53* isogenic AML cell lines (6). These cell lines harbor various *TP53* alleles comprising WT (+/+), monoallelic null (+/−), biallelic null (−/−), monoallelic missense (R248Q/+), and compound monoallelic missense and null mutations (R248Q/−), allowing us to directly compare the functional consequences of the different allelic configurations on canonical WT p53 functions (**Fig. 1A**). Upon treatment with the DNA-damaging chemotherapeutic Dauno to activate p53, we observed induction of p21, G1 arrest, and increased apoptosis in cells with +/+ (**Fig. 1B–D**). Although cells with +/− alleles had a significantly attenuated cell cycle and apoptotic response, its magnitude was only small (**Fig. 1B–D**). These WT p53-mediated responses were heavily impaired or completely lacking in cells with −/− or R248Q/− alleles. Notably, R248Q/+ cells showed a response that was indistinguishable to that observed in cells with R248Q/− or −/− alleles (**Fig. 1B–D**). Accordingly, cells with −/−, R248Q/−, or R248Q/+ alleles exhibited strong resistance to several commonly used chemotherapeutics as well as the MDM2 inhibitor Nutlin-3a, resulting in a competitive advantage over cells with +/+ or +/− alleles when tested in *in vitro* competition assays (**Fig. 1E–G**). The competitive fitness of cells with −/−, R248Q/−, or R248Q/+ relative to each other was comparable (**Fig. 1G**). Moreover, clonogenic potential upon treatment with nutlin-3a was reduced in cells harboring +/+ or +/− alleles but maintained in cells with −/−, R248Q/+, or R248Q/− alleles (**Fig. 1H** and **I**). Finally, NSG mice engrafted with MOLM13-*TP53* isogenic AML cells carrying −/−, R248Q/+, or R248Q/− alleles showed resistance to treatment with the MDM2 inhibitor idasanutlin, increased leukemic burden, and rapidly succumbed to the disease, whereas mice xenografted with cells with +/+ or +/− alleles had reduced leukemic burden and significantly prolonged survival (**Fig. 1J** and **K**; Supplementary Fig. S1A). Altogether, these data demonstrate a strong DNE of the R248Q missense variant on WT p53.

The presence of R248Q greatly impairs WT p53's ability to bind to DNA and to transactivate target gene expression

To investigate the mechanism by which the presence of R248Q inhibits WT p53 in cells with monoallelic missense mutations (R248Q/+), we first tested the ability of R248Q to translocate to the nucleus in the steady-state and following p53 activation by Dauno. Whereas cells with +/+, +/−, or −/− *TP53* alleles lacked relevant levels of p53 in DMSO controls, cells with R248Q/+ or R248Q/− alleles showed a p53 signal in the nucleus (Supplementary Fig. S2A). However, upon Dauno treatment, p53 could be strongly detected in all allelic states except for −/− (**Fig. 2A**). These results indicate that R248Q retains the ability to translocate to the nucleus similar to WT p53, ruling out the possibility that R248Q sequesters WT p53 in the cytoplasm and thereby inhibiting WT p53's transcriptional activity. We next performed ChIP sequencing in the steady-state (DMSO) or following p53 activation (Dauno) to test both the capacity of R248Q itself to bind to DNA as well as its effect on WT p53's DNA-binding abilities (**Fig. 2B–D**). First, we assessed the global enrichment of

(*Continued*.) K562-*TP53*^{null} AML cell lines lentivirally transduced to stably express full-length R248Q, tetramerization-deficient R248Q (R248Q-L344A), or dimerization-deficient R248Q (R248Q-L344P or R248Q-OD lacking the OD of p53) were treated for 3 hours with either DMSO or 100 nmol/L Dauno. Glutaraldehyde-fixed whole-cell protein lysates were separated on a polyacrylamide gel and immunoblotted for p53 ($n = 3$ independent experiments; representative blots are shown). **C,** Experimental schematic depicting the general principle of the flow cytometry–based FRET assay in K562-*TP53*^{null} AML cells. For experimental details, please refer to the Materials and Methods. **D,** Representative FACS plots showing results of the FRET assay in K562-*TP53*^{null} AML cells for the interaction between WT monomers (top), or WT and R248Q monomers (bottom). FRET donor and acceptor plasmids encoding p53 WT or R248Q variants either oligomerization-proficient (WT) or -deficient (WT-L344A, WT-L344P, or WT-OD) were co-electroporated into K562-*TP53*^{null} AML cells, followed by FRET measurement (FRET fluorescence measured using the 525/50-nm detector). **E,** Pooled results of the FRET assays in K562-*TP53*^{null} AML cells ($n = 3$ independent experiments). Bar graphs represent averages. Error bars, SD. ***, $P \le 0.001$; ****, $P \le 0.0001$, one-way ANOVA, Tukey multiple comparison. **F,** Experimental schematic and pooled results of the transcriptional reporter assay in K562-*TP53*^{null}-p21-GFP cells electroporated with plasmids encoding oligomerization-proficient or -deficient WT p53 variants ($n = 3$ independent experiments). Bar graphs represent averages. Error bars, SEM. *, $P \le 0.05$; **, $P \le 0.01$; ****, $P \le 0.0001$, one-way ANOVA, Tukey multiple comparison. **G,** Experimental schematic and pooled results of the transcriptional reporter assay in K562-*TP53*^{WT}-p21-GFP cells electroporated with pRK5 plasmids encoding oligomerization-proficient or -deficient R248Q p53 variants ($n = 3$ independent experiments). Bar graphs represent averages. Error bars, SEM. **, $P \le 0.01$; ****, $P \le 0.0001$, one-way ANOVA, Tukey multiple comparison. **H,** Quantification of the bioluminescent signal (i.e., total flux per second) for each group of mice 12 and 16 days after sublethal irradiation and subsequent injection with MOLM13-*TP53*$^{+/-}$-GFP-luciferase AML cell lines overexpressing either R248Q (WT + R248Q) or oligomerization-deficient R248Q-L344P (WT + R248Q-L344P). Following, mice were treated with idasanutlin (Ida, 25 mg/kg of BW per day) or vehicle (Veh) for seven consecutive days ($n = 7$ animals per group). Symbols represent averages. Error bars, SD. ***, $P \le 0.001$, Mann–Whitney test. **I,** Survival analysis of NSG mice engrafted with MOLM13-*TP53*$^{+/-}$-GFP-luciferase AML cell lines overexpressing either R248Q (WT + R248Q) or R248Q-L344P (WT + R248Q-L344P) and treated with idasanutlin (25 mg/kg of BW per day) or vehicle for seven consecutive days ($n = 7$ animals per group). ****, $P \le 0.0001$, Kaplan–Meier simple survival analysis. **J,** Experimental schematic and pooled results of the transcriptional reporter assay in K562-*TP53*^{R248Q}-p21-GFP cells electroporated with the pRK5 plasmid encoding oligomerization-proficient WT p53 variant ($n = 3$ independent experiments). Bar graphs represent averages. Error bars, SEM. ****, $P \le 0.0001$, Welch *t* test. CNTR, control; FRET-Acc, FRET acceptor; FRET-Don, FRET donor. ns, nonsignificant.

p53 binding to transcriptional start site (TSS)- proximal regions in cells with +/+, +/−, R248Q/+, or R248Q/− alleles relative to cells with −/− alleles that served as control (**Fig. 2B**). Whereas cells with R248Q/− alleles lacked relevant DNA binding, cells with at least one WT allele (i.e., +/+, +/−, or R248Q/+) showed readily detectable binding to TSS regions. However, upon Dauno treatment, TSS binding was heavily impaired in cells with R248Q/+ alleles as compared with cells with +/+ or +/− alleles (**Fig. 2B**). Moreover, individual DNA-binding peaks identified in cells with +/+, +/−, or R248Q/+ alleles, which largely overlap with few to no R248Q-specific peaks, indicate that R248Q itself not only loses the ability to bind to canonical p53 target genes but also does not acquire *de novo* DNA-binding sites (**Fig. 2C** and **D**). Last, we validated whether binding of p53 to TSS regions would lead to expression of the corresponding genes for the two canonical p53 targets, *CDKN1A* and *MDM2* (**Fig. 2D** and **E**). This was indeed the case for cells with +/+ and +/− alleles. However, although there was preserved binding to the TSS region of *MDM2* in cells with R248Q/+ alleles in DMSO controls and to a lesser extent even upon Dauno treatment, there was no detectable *MDM2* transcript expression (**Fig. 2D** and **E**).

Collectively, these data demonstrate that R248Q exerts a DNE on WT p53 in cells with monoallelic missense mutations by impairing the ability of WT p53 to bind to promoter DNA and to transactivate expression of target genes.

Oligomerization between R248Q and WT p53 is required for the DNE

Next, we set out to investigate the molecular mechanism of the DNE. Given that p53 is transcriptionally active only in its tetrameric state, we hypothesized that formation of heterotetramers between R248Q and WT p53 is critical for the DNE. We first addressed whether R248Q itself is able to form homotetramers. To this end, we performed glutaraldehyde fixation of protein lysates of isogenic MOLM13-*TP53* cells followed by Western blotting (**Fig. 3A**). We readily detected p53 monomers, dimers, and tetramers not only in isogenic MOLM13-*TP53* cells carrying at least one WT *TP53* allele (+/+, +/−, or R248Q/+) but also in MOLM13-*TP53* cells expressing exclusively the R248Q missense variant (R248Q/−), indicating that, indeed, R248Q is capable of oligomerizing similar to WT p53 (**Fig. 3A**).

Whether heterotetramerization between R248Q and WT p53 occurs in MOLM13-*TP53* cells with monoallelic missense mutations (R248Q/+) is, however, not directly verifiable as both p53 variants only differ in a single amino acid, thereby precluding direct proteomic assessments. We, therefore, used MOLM13-$TP53^{null}$ and K562-$TP53^{null}$ cells to express exogenous R248Q variants that are either largely tetramerization-deficient but can still form dimers (L344A) or that are oligomerization-deficient either via introducing the L344P missense mutation or by deleting p53's C-terminal OD (**Fig. 3B**). Using these oligomerization-deficient p53 variants as well as their oligomerization-proficient controls in a previously described flow cytometry–based FRET assay (14) allowed us to assess whether there is direct physical interaction between R248Q and WT p53 and thus likely formation of heterotetramers. To this end, the various p53 variants were C-terminally labeled in all possible combinations with three different fluorochromes, i.e., Amber (nonfluorescent control to set the flow cytometry gates), ECFP (FRET donor), and mVenus (FRET acceptor), followed by co-electroporation of plasmids into K562-$TP53^{null}$ cells and subsequent FACS-FRET measurements (**Fig. 3C**). As expected, when only oligomerization-proficient WT-ECFP and WT-mVenus, or R248Q-ECFP and R248Q-mVenus variants were assessed, a strong FRET signal was observed (**Fig. 3D** and **E**; Supplementary Fig. S3A), indicating generation of homotetramers consisting of either only WT or only R248Q monomers, respectively. However, upon co-electroporation of oligomerization-deficient p53 variants, the FRET signal was strongly reduced to almost background levels (**Fig. 3D** and **E**; Supplementary Fig. S3A), thereby independently confirming that the FRET signal is due to direct physical protein–protein interactions. Intriguingly, the FRET signal was already heavily reduced (>75%) upon prevention of tetramerization but retention of dimerization capabilities, suggesting that tetramers consisting of homodimers (i.e., WT:WT or R248Q:R248Q dimers) but not heterodimers (i.e., WT:R248Q dimers) are preferentially formed under unperturbed conditions. This notion was proposed by previous studies using *in vitro* translation assays postulating a dimer:dimer topology model of p53 tetramerization (15, 16). We could confirm such a model by conducting another set of FRET assays. In line with our previous results (**Fig. 3D** and **E**; Supplementary Fig. S3A), preventing tetramerization of the p53 variant acting as FRET acceptor led to a heavily (>75%) reduced FRET signal that was, however and surprisingly, rescued by concomitant prevention of tetramerization of the p53 variant acting as the FRET donor (Supplementary Fig. S3B). These results strongly suggest that under normal conditions, homodimers rarely dissociate, and thus tetramers are largely formed upon dimerization of homodimers (i.e., either WT:WT or R248Q:R248Q homodimers; Supplementary Fig. S3C). Altogether, above data clearly demonstrate that WT and R248Q are capable of forming heterotetramers.

We next assessed the transcriptional activity of heterotetramers. To this end, we CRISPR-engineered K562 cell lines to carry $TP53^{WT}$, $TP53^{null}$, and $TP53^{R248Q}$ alleles while simultaneously tagging the endogenous *CDKN1A* locus, encoding for the canonical p53 target p21, with GFP allowing us to measure p53's transcriptional activity by flow cytometry. As expected, electroporation of plasmids encoding WT p53 into reporter cells with endogenous $TP53^{null}$ (K562-$TP53^{null}$-p21-GFP) followed by nutlin-3a treatment to activate p53 led to detection of the p21-GFP reporter signal (**Fig. 3F**; Supplementary Fig. S3D). However, the p21-GFP signal was strongly attenuated upon electroporation of oligomerization-deficient WT p53 confirming that only WT p53 homotetramers are fully transcriptionally active (**Fig. 3F**; Supplementary Fig. S3D). By contrast, electroporation of plasmids encoding the R248Q variant into reporter cells with endogenous $TP53^{WT}$ (K562-$TP53^{WT}$-p21-GFP) resulted in suppression of the p21-GFP reporter signal, demonstrating the DNE exerted by R248Q on WT p53 (**Fig. 3G**; Supplementary Fig. S3E). When oligomerization-deficient R248Q variants were electroporated, the p21-GFP reporter signal was fully rescued (**Fig. 3G**; Supplementary Fig. S3E). To test whether heterotetramerization is required for the DNE *in vivo*, we xenografted NSG mice with MOLM13-*TP53* cells carrying a WT allele and expressing either tetramerization-proficient (R248Q) or tetramerization-deficient (R248Q-L344P) R248Q variants and treated them with either vehicle or idasanutlin. Leukemic burden was reduced and survival was prolonged in idasanutlin-treated mice with cells harboring R248Q-L344P (**Fig. 3H** and **I**; Supplementary Fig. S4A). Collectively, these data demonstrate that the DNE critically depends on R248Q's ability to form heterotetramers with WT p53 monomers *in vitro* and *in vivo*.

Notably, electroporation of plasmids encoding WT p53 into cells with endogenous $TP53^{R248Q}$ (K562-$TP53^{R248Q}$-p21-GFP) almost fully restored the p21-GFP reporter signal (**Fig. 3J**; Supplementary Fig. S4B). These somewhat surprising results suggest that the DNE of R248Q can be overcome by overexpression of WT p53, thereby increasing the WT:R248Q ratio.

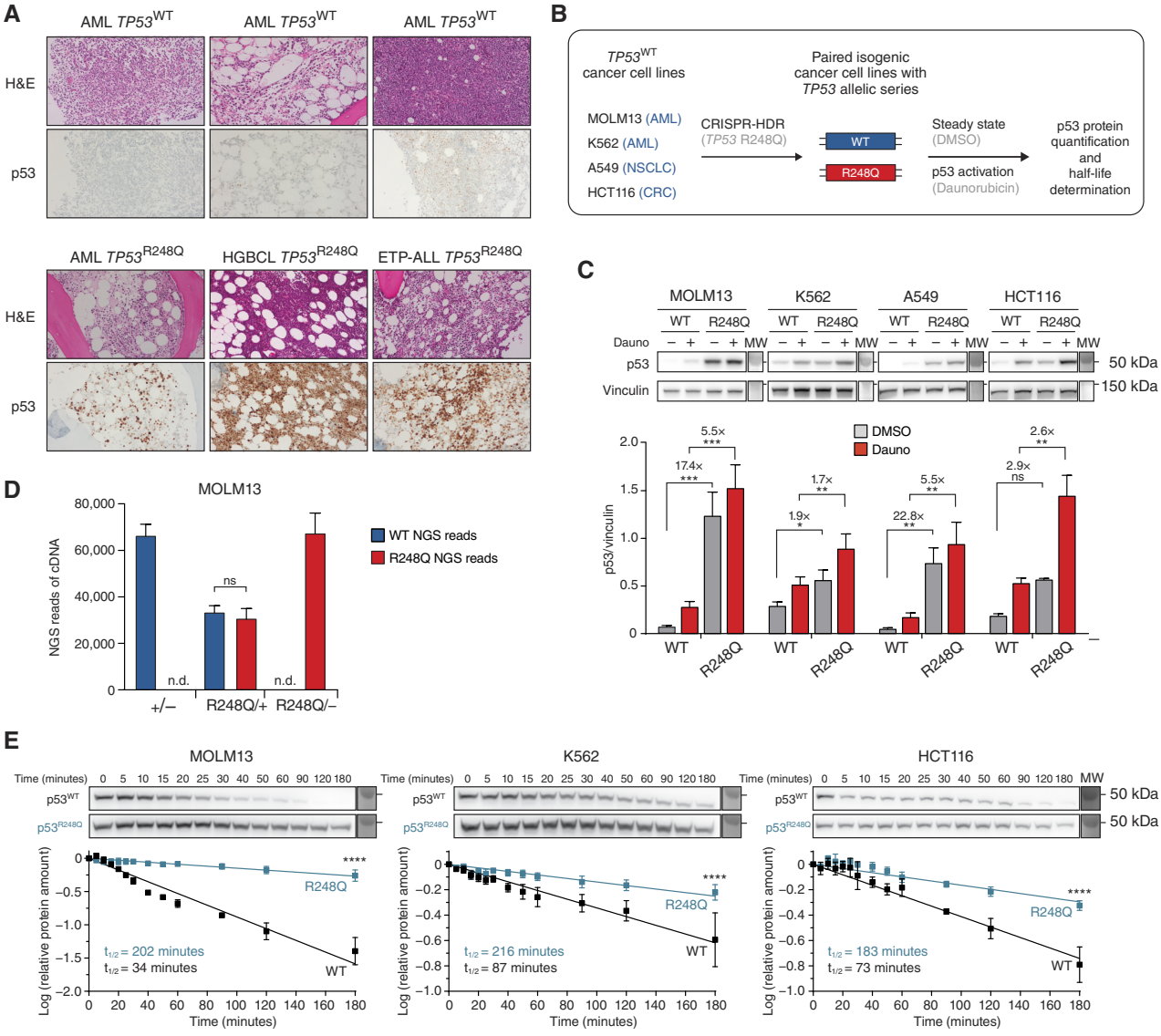

Figure 4.

The longer protein half-life of R248Q leads to an increase of the R248Q:WT ratio. **A,** Bone marrow biopsies of patients with *TP53*^{WT} or *TP53*^{R248Q}-mutant AML, high-grade B-cell lymphoma (HGBCL), or early T precursor lymphoblastic leukemia (ETP-ALL) stained with hematoxylin and eosin (H&E) and p53 IHC ($n = 6$ representative images; ×100 magnification) show strong nuclear p53 staining in neoplastic cells of *TP53*^{R248Q} mutated cases. **B,** Experimental schematic for the CRISPR/Ca9-mediated generation of human isogenic cancer cell lines with *TP53* WT or R248Q alleles and their subsequent use for p53 quantification and half-life determination as shown in **C** and **E**. CRC, colorectal cancer; CRISPR-HDR, CRISPR-Cas9–mediated homology-directed repair; NSCLC, non–small cell lung cancer. **C,** Whole-cell lysates of isogenic MOLM13-*TP53*, K562-*TP53*, A549-*TP53*, and HCT116-*TP53* isogenic cell lines with WT and R248Q alleles treated for 6 hours with either DMSO or 100 nM Dauno were separated on a polyacrylamide gel and immunoblotted for p53 and vinculin. P53 was quantified via ImageJ software using vinculin to normalize p53 levels ($n = 3$–4 independent experiments; representative blots are shown). Bar graphs represent averages. Error bars, SEM. *, $P \leq 0.05$; **, $P \leq 0.01$; ***, $P \leq 0.001$, two-way ANOVA, Tukey multiple comparison. **D,** NGS of cDNA from isogenic MOLM13-*TP53* AML cell lines of the indicated genotypes. Number of NGS reads supporting the WT (gray) or R248Q (blue) allele are shown ($n = 3$ independent experiments). Bar graphs represent averages. Error bars, SD. Two-way ANOVA, Tukey multiple comparison. ns, nonsignificant; n.d., not detectable. **E,** Half-life determination of p53 WT and R248Q in untreated isogenic MOLM13-*TP53*, K562-*TP53*, A549-*TP53*, and HCT116-*TP53* isogenic cell lines. Whole-cell lysates of cycloheximide-treated cells were collected at the indicated time points and separated on a polyacrylamide gel and immunoblotted for p53 and vinculin. p53 was quantified using ImageJ software ($n = 3$–4 independent experiments; representative blots are shown). Error bars, SEM. ****, $P \leq 0.0001$, Mann–Whitney test.

R248Q has a longer protein half-life, leading to strong accumulation relative to WT p53

The observation that overexpression of WT p53 can overcome the dominant-negative activity of R248Q prompted us to reassess the long-standing observation that cancer-associated p53 missense variants tend to be more abundant in cancer cells than WT p53. In fact, whereas WT p53 is kept at low to undetectable levels in unstressed normal tissues as well as in cancer cells with WT p53 (17,

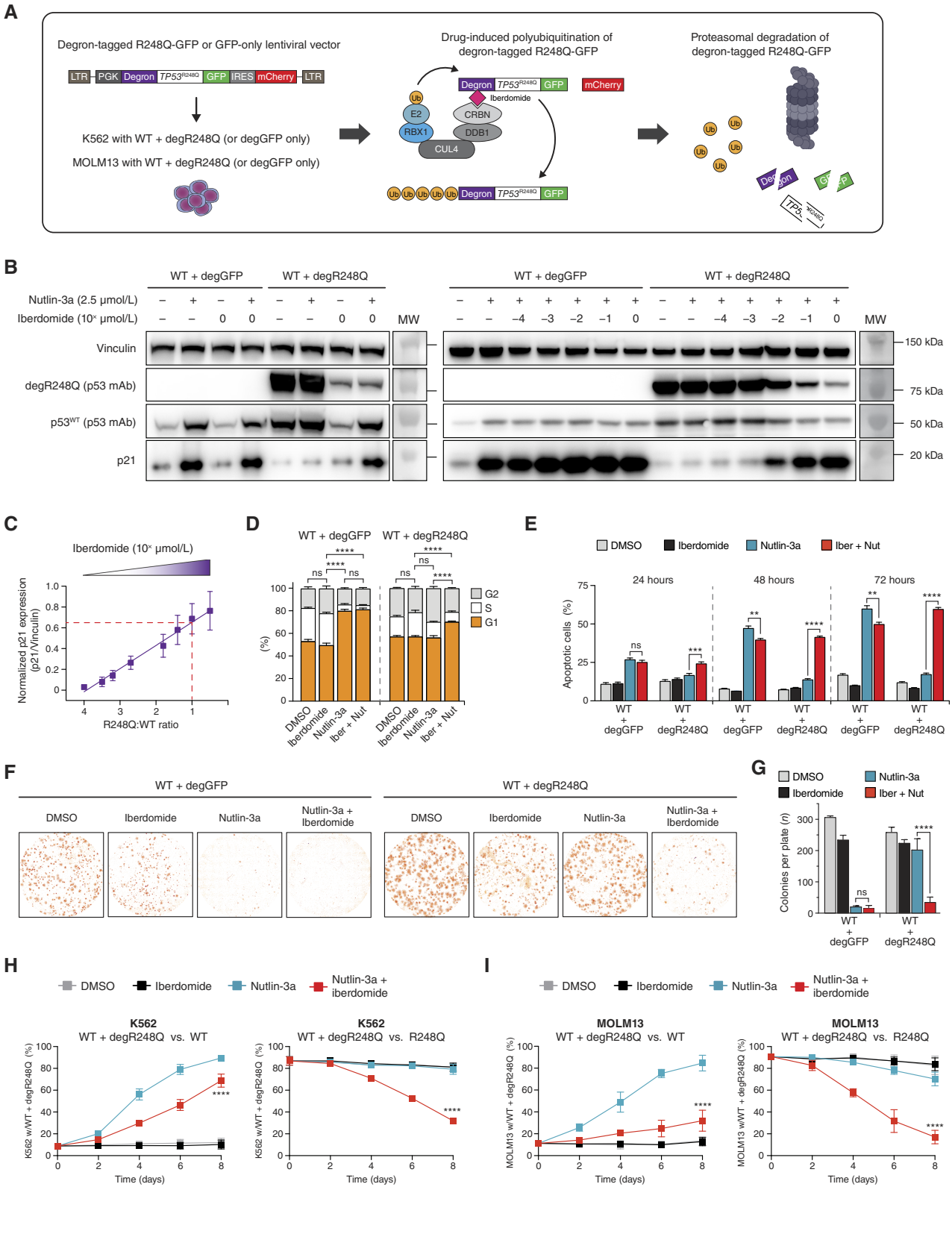

18), *TP53*-mutant cancer cells often show a readily detectable p53 signal on IHC – a histopathologic feature that is often used in clinical routine diagnostics as a surrogate marker for the presence of *TP53* missense mutations (**Fig. 4A**; refs. 19, 20). However, this observation does not prove that the R248Q variant possesses the inherent predisposition to increase in abundance because this observation could simply be caused by cell-autonomous pathways that are present in cancer cells with *TP53* mutations but absent in those with WT *TP53*. Therefore, to investigate whether the R248Q missense variant has the intrinsic property of accumulating in cancer cells, we used precise CRISPR/Cas9-mediated genome editing to generate additional isogenic pairs of cancer cell lines expressing R248Q or WT p53 from the endogenous *TP53* locus. We generated a total of four different isogenic cell lines of various tissue origins (MOLM13, AML; K562, chronic myeloid leukemia; A549, non–small cell lung cancer; HCT116, colorectal carcinoma; **Fig. 4B**). Indeed, in all these isogenic cell line pairs treated with Dauno, R248Q showed increased levels relative to WT p53 in the range of 1.7- to 5.5-fold (**Fig. 4C**). Next, we sought to determine whether this phenomenon is regulated on the transcriptional or (post)translational level. To this end, we RT-PCR amplified an amplicon spanning the R248 residue (c.743G) followed by NGS in MOLM13 cells with R248Q/+ as well as in MOLM13 with R248Q/− or +/− alleles as controls. We observed approximately equal numbers of WT and R248Q NGS reads in MOLM13 with R248Q/+ alleles. By contrast, there were about twice as many WT but no R248Q NGS reads and twice as many R248Q but no WT NGS reads in MOLM13 cells with +/− or R248Q/− alleles, respectively. These data indicate that mRNA translated from the R248Q allele is not more abundant than WT p53 mRNA (**Fig. 4D**) and thus does not explain higher protein levels of R248Q as compared with WT p53.

We then determined the protein half-lives of WT p53 and the R248Q missense variant using cycloheximide treatment followed by Western blotting in isogenic pairs of cell lines with WT or R248Q *TP53* alleles only. The protein half-life of WT p53 in MOLM13, K562, or HCT116 cell lines ranged between 34 and 87 minutes (**Fig. 4E**). By contrast, in their isogenic counterparts R248Q had a markedly increased protein half-life of 183 to 216 minutes (**Fig. 4E**), demonstrating that, indeed, R248Q accumulates due to increased protein stability.

Based on these findings, we hypothesized that the ability of the R248Q variant to accumulate to supraphysiologic levels in cancer cells may not merely be an epiphenomenon but rather a pivotal attribute contributing to the DNE.

A supraphysiologic protein abundance of R248Q is required for the DNE

To test above hypothesis, we set out to generate an experimental model system that would allow us to precisely control the protein level of the R248Q variant in cells that also express WT p53 to eventually determine the relationship between the R248Q:WT ratio and the transcriptional activity of WT p53 (**Fig. 5A**). To this end, we utilized a previously described degron-tagging system (12, 21) to generate a LV expression construct carrying the full-length cDNA of R248Q fused to a degron tag and a GFP tag on its N- and C-terminus, respectively. Furthermore, this construct was linked to mCherry via an IRES. When expressed in cells with an endogenous *TP53*^{WT} allele, the exogenous R248Q-GFP variant exerts a DNE on WT p53 expressed from the endogenous locus (**Fig. 5B**). The promoter of the LV construct was chosen to recapitulate the previously established R248Q:WT ratio at baseline of about 3- to 4-fold more R248Q than WT p53 (**Fig. 4C**). Upon treatment with thalidomide derivatives acting as proximity-inducing molecular glues involving the N-terminal degron, polyubiquitination of the R248Q-GFP fusion variant by the cereblon complex is triggered, resulting in its proteasomal degradation. Given that the R248Q-GFP fusion and mCherry are being expressed from the same mRNA but separated by an IRES, mCherry is nondegradable, and the protein levels of the R248Q variant can be precisely calculated on the single-cell level based on the GFP/mCherry ratio (**Fig. 5A**; Supplementary Fig. S5A and S5B). We tested several thalidomide derivatives, with iberdomide being the most efficient molecular glue degrader in this system

Figure 5.

A supraphysiologic protein abundance of R248Q is required for the DNE. **A,** Experimental schematic showing the principle of the p53 target degradation assay. **B,** Whole-cell lysates of iberdomide- and/or nutlin-3a–treated K562 cells with *TP53*^{WT} and degR248Q or K562 cells with *TP53*^{WT} and degGFP were separated on a polyacrylamide gel and immunoblotted for p53, p21, and vinculin ($n = 3$ independent experiments; one representative blot is shown). **C,** Correlation between the WT p53 transcriptional activity as determined by the normalized p21/vinculin and the R248Q/WT ratio in K562 cells with *TP53*^{WT} and degR248Q. Cells were treated with 2.5 μmol/L nutlin-3a and increasing concentrations of iberdomide, whole-cell lysates were prepared, run on a polyacrylamide gel, immunoblotted for p53, p21, and vinculin, and bands were quantified using ImageJ software ($n = 3$ independent experiments, pooled data, including averages and SEM are shown). **D,** Cell-cycle distribution of MOLM13 cells with WT *TP53* and degR248Q or MOLM13 cells with WT *TP53* and degGFP cells in the absence or presence of 1 μmol/L iberdomide and/or 2.5 μmol/L nutlin-3a for 24 hours as determined by CytoPhase Violet staining ($n = 3$ independent experiments). Bar graphs represent averages. Error bars, SEM. ****, $P \leq 0.0001$, one-way ANOVA, Tukey multiple comparison. **E,** Fraction of apoptotic MOLM13 cells with WT *TP53* and degR248Q or degGFP as determined by Annexin V staining in the absence or presence of 1 μmol/L iberdomide and/or 2.5 μmol/L nutlin-3a for 24 to 72 hours ($n = 3$ independent experiments). Bar graphs represent averages. Error bars, SEM. **, $P \leq 0.01$; ***, $P \leq 0.001$; ****, $P \leq 0.0001$, two-way ANOVA, Tukey multiple comparison. **F,** Representative images of a colony-forming unit assay was performed in MOLM13 cells with WT *TP53* and degR248Q or degGFP in methylcellulose-based medium containing DMSO, 5 μmol/L iberdomide, and/or 2.5 μmol/L nutlin-3a. After 7 days, images were taken using a Leica DMI6000 B inverted microscope, and analysis was performed using the Colony Area ImageJ plugin, followed by manual counting of the colonies (representative images of $n = 3$ independent experiments). **G,** Summary of counted colonies from the colony-forming unit assay as described in **F** ($n = 3$ independent experiments). Bar graphs represent averages. Error bars, SEM. ****, $P \leq 0.0001$, one-way ANOVA, Tukey multiple comparison. **H,** Results of *in vitro* competition assays of K562 cells with WT *TP53* and degR248Q cocultured together with isogenic K562-*TP53*^{WT} cells (left) or K562-*TP53*^{R248Q} cells (right) in the absence or presence of 2.5 μmol/L nutlin-3a and/or 1 μmol/L iberdomide. The relative fractions of each genotype were determined by flow cytometry every other day for 8 days ($n = 3$ independent experiments). Averages are shown. Error bars, SD. ****, $P \leq 0.0001$, unpaired *t* test. **I,** The results of *in vitro* competition assays of MOLM13 cells with WT *TP53* and degR248Q cocultured together with isogenic MOLM13 cells with WT *TP53* (left) or MOLM13 cells with R248Q (right) in the absence or presence of 2.5 μmol/L nutlin-3a and/or 1 μmol/L iberdomide. The relative fractions of each genotype were determined by flow cytometry every other day for 8 days ($n = 3$ independent experiments). Symbols indicate averages. Error bars, SD. ****, $P \leq 0.0001$, unpaired *t* test; ns, nonsignificant.

(Supplementary Fig. S5A and S5B). Treatment with iberdomide led to a dose-dependent decrease of R248Q levels while leaving the level of endogenous WT p53 largely unaffected. Concomitantly, there was a gradual increase in p21 expression, demonstrating restoration of WT p53's transcriptional activity upon degradation of R248Q (**Fig. 5B**). We then quantified the R248Q:WT ratio and correlated it with the normalized p21 expression levels. At a R248Q:WT ratio of about 1, WT p53's transcriptional activity, as measured by expression of p21, was only reduced to about 65%. By contrast, full suppression of p21 expression and thus a complete DNE was only observed at markedly increased R248Q:WT ratios of 3 to 4:1 (**Fig. 5C**), which corresponds well to the naturally occurring degree of R248Q protein accumulation as determined in isogenic cell line pairs (**Fig. 4C**).

Next, we investigated whether iberdomide-induced degradation of R248Q and subsequent restoration and activation of WT p53 activity would translate into an antiproliferative, therapeutic effect. First, we tested cell-cycle distribution, apoptosis, and clonogenic potential in MOLM13-*TP53* cells carrying a WT allele and expressing either degGFP or degR248Q. Iberdomide-induced degradation of R248Q together with nutlin-3a treatment of MOLM13-*TP53* cells carrying a WT allele and expressing degR248Q restored WT p53 activity, as indicated by an increase of cells in G1, strong induction of apoptosis, and reduced clonogenic potential, whereas either DMSO, iberdomide, or nutlin-3a treatment alone had no relevant effect (**Fig. 5D–G**). Of note, in MOLM13-*TP53* cells carrying a WT allele and expressing degGFP no DNE was observed, and thus, cells exhibited WT p53 functionality upon nutlin-3a treatment without additional relevant effects by iberdomide (**Fig. 5D–G**).

To test, whether restored WT p53 would translate into a selective antiproliferative effect, we set up *in vitro* competition assays of K562 or MOLM13 cell lines with a WT p53 allele and degR248Q versus their isogenic counterparts with only WT p53 or R248Q alleles (**Fig. 5H** and **I**). As expected, in the absence of iberdomide, nutlin-3a treatment led to a rapid outgrowth of cells with WT p53 and degR248Q over cells with WT p53 only (**Fig. 5H** and **I**, left) or no effect compared with cells with R248Q only (**Fig. 5H** and **I**, right), thereby demonstrating the DNE. However, upon combinatorial idasanutlin/iberdomide treatment, and thus degradation of R248Q, cells with a WT p53 and degR248Q lost their competitive advantage over cells with WT p53 only (**Fig. 5H** and **I**, left) or gained a competitive disadvantage as compared with cells with R248Q only (**Fig. 5H** and **I**, right). These data not only independently validate the DNE of R248Q over WT p53 but reveal that the DNE can be overcome by lowering the R248Q:WT ratio via degradation of R248Q, resulting in restoration of WT p53 activity and thus a strong antiproliferative effect *in vitro*.

Lowering the increased R248Q:WT protein ratio shows striking therapeutic efficacy *in vivo*

Last, we wanted to investigate whether degradation of R248Q in cells with a WT *TP53* allele would result in a therapeutic benefit *in vivo*. To this end, we generated MOLM13-*TP53*$^{+/-}$ cells expressing either degradable BFP or degR248Q. Of note, cells also expressed GFP and luciferase to allow confirmation of engraftment as well as noninvasive assessment of leukemic burden by IVIS imaging, respectively. Following confirmation of engraftment, mice were treated with vehicle, idasanutlin, and/or iberdomide and monitored for leukemic burden and survival (**Fig. 6A**). Mice engrafted with MOLM13-*TP53*$^{+/-}$ cells expressing degR248Q and treated with vehicle, idasanutlin, or iberdomide showed rapidly progressing AML and succumbed to their disease within 20 to 25 days (**Fig. 6B–D**). By contrast, mice treated with a combination of iberdomide and idasanutlin had significantly reduced leukemic burden and prolonged survival, with some mice even achieving long-term disease control (**Fig. 6B–D**). Notably, mice engrafted with MOLM13-*TP53*$^{+-}$ cells expressing degradable BFP did not show evidence of a DNE, and thus, the combined treatment of iberdomide and idasanutlin did not have an additive or synergistic therapeutic effect compared with treatment with idasanutlin alone. Altogether, these data demonstrate that targeted degradation of R248Q, thereby lowering the R248Q:WT ratio, can have a striking therapeutic effect *in vivo*.

Discussion

In this study, we have elucidated fundamental aspects of the DNE that the frequent hotspot p53 missense variant R248Q exerts on WT p53 in cells with monoallelic *TP53*^{R248Q} mutations. We demonstrate that R248Q and WT p53 directly interact to form heterotetramers that translocate to the nucleus, in which they, however, fail to bind to DNA to transactivate gene expression, as suggested previously (22). However, our findings reveal that equimolar amounts of R248Q and WT p53 would not suffice to exert a relevant DNE, i.e., to decrease WT p53 transcriptional activity below that observed in cells with monoallelic null mutations. By contrast, supraphysiologic levels of R248Q – as a consequence of its markedly prolonged protein half-life – are critically required for the DNE (**Fig. 7A**, left). This surprising finding sheds new light on the long-standing observation of accumulation of p53, as determined by IHC, in cancer cells with *TP53* missense mutations. Rather than being merely an epiphenomenon and useful surrogate marker for *TP53* missense mutations in clinical routine diagnostics (19, 20), supraphysiologic p53 accumulation is, in fact, one of the crucial biochemical properties of R248Q and likely other biochemically similar missense p53 variants, thereby contributing to its DNE.

It is tempting to conceive a model of the DNE, in which an increased R248Q:WT ratio in cells with monoallelic R248Q missense mutations (R248Q/+) shifts the stoichiometry of WT homotetramers (transcriptionally active) markedly toward R248Q:WT heterotetramers and R248Q homotetramers that are transcriptionally impaired (**Fig. 7B**), as suggested previously (23). In this regard, previous biochemical studies using superstable p53 mutants in cell-free *in vitro* assays have suggested that p53 tetramers do not form from freely interacting p53 monomers (**Fig. 7B**, top) but rather through dimerization of dimers that are already formed cotranslationally on the polysome (**Fig. 7B**, bottom; refs. 15, 16). Our results obtained in cellular *in vivo* models, indeed, support such a dimer:dimer topology model of p53 tetramerization. First, tetramerization-deficient variants show a strong (>75%) loss of the FRET signal, similar to the FRET signal observed in dimerization-deficient variants. Second, this loss of FRET signal is rescued to approximately 50% of the baseline FRET signal upon concomitant prevention of tetramerization of both the p53 variant acting as the FRET donor as well as the p53 variant acting as the FRET acceptor. Only under such conditions, in which tetramers cannot be formed anymore, homodimers seem to dissociate and redimerize to form heterodimers, thereby regaining the FRET signal up to the expected 50% of baseline values (Supplementary Fig. S3B and S3C). Altogether, previous and our new results heavily argue against the existence of R248Q:WT heterodimers under normal, unperturbed conditions but only of either WT or R248Q homodimers. Such a dimer:dimer topology model and assuming equal amounts of WT

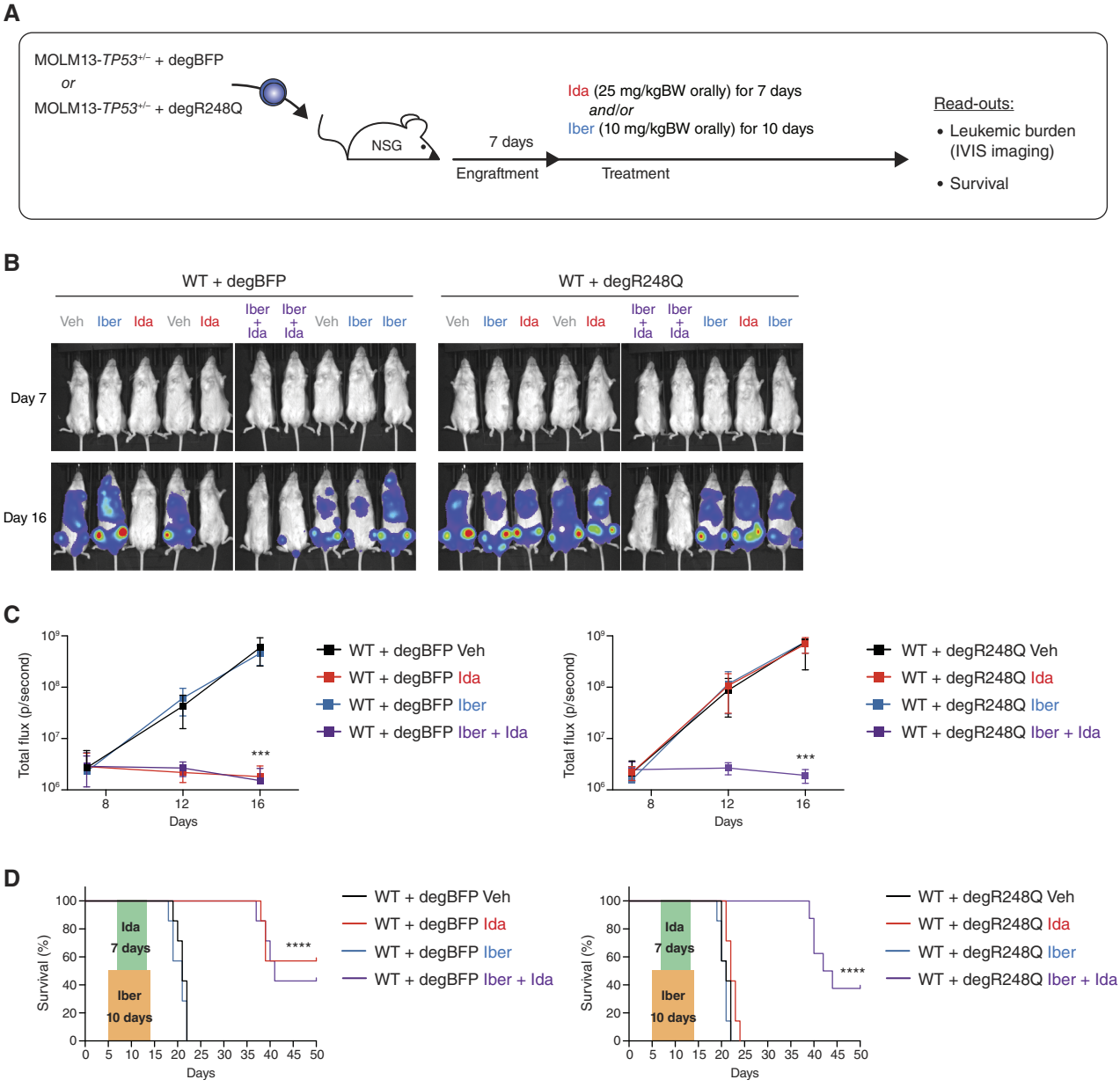

Figure 6.

Therapeutic efficacy of lowering the increased R248Q:WT protein ratio *in vivo*. **A,** Experimental workflow for *in vivo* p53-targeted R248Q degradation xenograft assay. MOLM13 cells with WT *TP53* with degradable BFP (degBFP) or R248Q (degR248Q) as well as GFP-luciferase were transplanted into sublethally irradiated NSG mice. After 5 to 7 days, treatment with vehicle (Veh), iberdomide (Iber), and/or idasanutlin (Ida) at the indicated concentrations was initiated and continued for 7 to 10 days, respectively. Leukemic burden was assessed by bioluminescent imaging 12 and 16 days after injection, and survival was monitored. **B,** Representative bioluminescent images of mice treated according to the experimental workflow depicted in **A**. **C,** Quantification of the bioluminescent signal (i.e., total flux per second) for each group of mice 12 and 16 days after sublethal irradiation and injection of MOLM13 cells with WT *TP53* and degR248Q or degBFP and GFP-luciferase. Mice were treated as described in **A** ($n = 7$ animals per group). Symbols represent averages. Error bars, SD. ***, $P \leq 0.001$, Mann–Whitney test. **D,** Survival analysis of NSG mice engrafted with MOLM13 cells with WT *TP53* and degR248Q or degBFP and GFP-luciferase and treated as described in **A** ($n = 7$ animals per group). ****, $P \leq 0.0001$, Kaplan–Meier simple survival analysis.

and R248Q homodimers as well as similar probabilities to form all three possible tetramers, 25% of all tetramers would still be WT homotetramers, and one would expect residual WT p53 transcriptional activity (**Fig. 7B**, bottom). By contrast, under the same assumptions but applying a model of free tetramerization of monomers, five different types of tetramers are theoretically possible, with only 1/16 (6.25%) of them being WT homotetramers (**Fig. 7B**, top). Consequently, one would expect a more pronounced impairment of WT p53 transcriptional activity. A heavily imbalanced stoichiometry in favor of

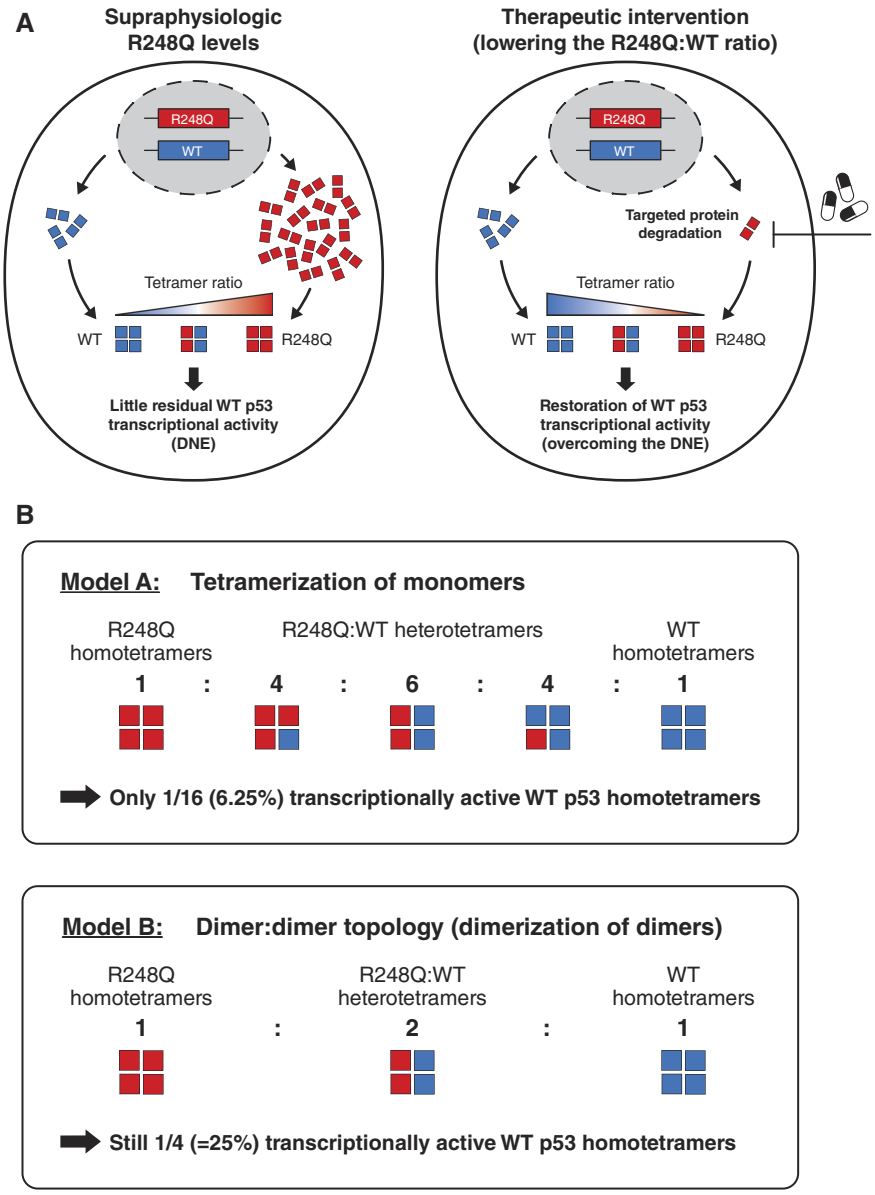

Figure 7.

Proposed models for DNE exerted by R248Q on WT p53. **A,** Visual summary of the findings of the present study demonstrating that the increased R248Q:WT ratio is a critical determinant of the DNE of R248Q and a putative therapeutic target. **B,** Hypothetical model (model A, top) and proposed model (model B, bottom) for the oligomerization of R248Q and WT p53 monomers in cells with monoallelic *TP53*^{R248Q} missense mutations based on the findings of the present study and refs. 11 and 12.

transcriptionally impaired R248Q:WT heterotetramers or R248Q homotetramers via increased R248Q abundance, as shown in this study, would, however, explain the complete absence of residual WT p53 activity, thereby reconciling previous and our current data.

It needs to be noted that the exact degree of R248Q accumulation, and thus, the strength of the DNE, may differ depending on the cellular and/or genomic context of the cancer type. In fact, it is likely that in most cancers, the DNE is incomplete, i.e., not fully suppressing WT p53 activity, as there is still a strong selective pressure for mutational inactivation of the remaining WT allele. However, the DNE may be particularly strong for the R248Q variant because previous studies in patients with germline *TP53* mutations (termed Li-Fraumeni syndrome) carrying the R248Q variant showed extraordinarily low frequencies of loss-of-heterozygosity (24).

Furthermore, whether all *TP53* missense mutations that exert a DNE do so because of heterotetramerization and supraphysiologic accumulation of the missense variant remains to be determined. Given the diverse biochemical properties of missense p53 variants (e.g., DNA contact vs. structural mutants; ref. 25) different DNE mechanisms may exist. Along these lines, whether highly unstable structural mutants that unfold at body temperature are able to heterotetramerize with WT p53 is, to our knowledge, unknown. Several other possible DNE mechanisms are conceivable based on reported biochemical properties of missense mutant p53, including the formation of prion-like aggregates inducing misfolding of WT p53 (26–28) and/or competing for cofactors required for normal WT p53 activity (29).

Importantly, the exact mechanism by which R248Q accumulates—whether it is an intrinsic biochemical property of R248Q or rather an indirect consequence—is incompletely understood (30) and will be the focus of future studies.

Finally, the DNE represents a promising therapeutic target. Pharmacologic approaches such as mutant-specific siRNAs (31, 32), identification of molecular glue degraders or proteolysis-targeting chimeras that specifically induce degradation of R248Q while leaving WT p53 intact (**Fig. 7A,** right), or preventing the accumulation of R248Q in the first place, could have a relevant therapeutic benefit in patients with cancer with monoallelic *TP53*^{R248Q} mutations or in the setting of cancer prevention such as in patients with Li-Fraumeni syndrome.

Authors' Disclosures

P.G. Miller reports personal fees from Foundation Medicine outside the submitted work. S.A. Armstrong reports personal fees from Accent Therapeutics, AstraZeneca, C4 Therapeutics, Hyku Therapeutics, Neomorph, Inc., and Stelexis Therapeutics and grants from Syndax Pharmaceuticals and Janssen Biotech outside the submitted work; in addition, S.A. Armstrong has a patent for "Menin inhibition in NPM1 AML" issued. B.L. Ebert reports grants from Novartis and Calico and personal fees from Neomorph, Exo Therapeutics, Skyhawk Therapeutics, and TenSixteen Bio outside the submitted work. S. Boettcher reports grants from the Swiss Cancer League, Helmut Horten Stiftung, Promedica Stiftung, and the Swiss National Science Foundation during the conduct of the study. No disclosures were reported by the other authors.

Authors' Contributions

N. Klemm: Conceptualization, resources, data curation, formal analysis, supervision, funding acquisition, investigation, visualization, methodology, writing–original draft, project administration, writing–review and editing. **R.R. Schimmer:** Data curation, formal analysis, investigation, visualization, methodology, writing–original draft, writing–review and editing. **N.K. Konrad:** Formal analysis, investigation, visualization, methodology. **F. Thelen:** Data curation, formal analysis, investigation, visualization, methodology, writing–review and editing. **J. Fullin:** Investigation, methodology, writing–review and editing. **E. Topçu:** Formal analysis, investigation, visualization, methodology, writing–review and editing. **C. Koch:** Investigation, methodology, writing–review and editing. **M. Treacy:** Investigation, visualization, methodology. **M.J. Leventhal:** Data curation, formal analysis, investigation, visualization, methodology. **M.M. Bühler:** Conceptualization, resources, data curation, formal analysis, investigation, visualization, methodology. **V. Lysenko:** Resources, formal analysis, investigation, methodology. **A.P. Theocharides:** Conceptualization, resources, supervision. **K.J. Kurppa:** Conceptualization, resources, supervision, methodology. **S. Balabanov:** Conceptualization, formal analysis, investigation, methodology. **T. Baubec:** Conceptualization, supervision. **A.V. Krivtsov:** Conceptualization, supervision. **P.G. Miller:** Conceptualization, formal analysis, supervision, investigation, methodology. **S.A. Armstrong:** Conceptualization, supervision. **B.L. Ebert:** Conceptualization, supervision, visualization. **M.G. Manz:** Conceptualization, formal analysis, supervision, investigation, visualization, methodology. **C. Nombela-Arrieta:** Conceptualization, resources, supervision. **S. Boettcher:** Conceptualization, resources, data curation, supervision, funding acquisition, investigation, visualization, methodology, writing–original draft, project administration, writing–review and editing.

Acknowledgments

This work was supported by research grants of the EHA Kick-off Grant (KOG-202209-02593) to F. Thelen, the KRAK-Physician Scientist Fellowship and the Jacques and Gloria Gossweiler Foundation to R.R. Schimmer, the NIH (K08-CA263181) to P.G. Miller, the Swiss National Science Foundation (310030_184747/1) to M.G. Manz, the Swiss National Science Foundation (310030_219699) to C. Nombela-Arrieta as well as research grants by the Swiss Cancer League (KFS-4885-08-2019), the Helmut Horten Foundation, the Promedica Foundation, and the Swiss National Science Foundation (310030_197562/1) to S. Boettcher.

Note

Supplementary data for this article are available at Cancer Research Online (http://cancerres.aacrjournals.org/).

Received April 5, 2024; revised December 15, 2024; accepted March 24, 2025; posted first March 31, 2025.

References

1. Kastenhuber ER, Lowe SW. Putting p53 in context. Cell 2017;170:1062–78.
2. Brosh R, Rotter V. When mutants gain new powers: news from the mutant p53 field. Nat Rev Cancer 2009;9:701–13.
3. Muller PA, Vousden KH. p53 mutations in cancer. Nat Cell Biol 2013;15:2–8.
4. Aubrey BJ, Janic A, Chen Y, Chang C, Lieschke EC, Diepstraten ST, et al. Mutant TRP53 exerts a target gene-selective dominant-negative effect to drive tumor development. Genes Dev 2018;32:1420–9.
5. Giacomelli AO, Yang X, Lintner RE, McFarland JM, Duby M, Kim J, et al. Mutational processes shape the landscape of TP53 mutations in human cancer. Nat Genet 2018;50:1381–7.
6. Boettcher S, Miller PG, Sharma R, McConkey M, Leventhal M, Krivtsov AV, et al. A dominant-negative effect drives selection of TP53 missense mutations in myeloid malignancies. Science 2019;365:599–604.
7. Redman-Rivera LN, Shaver TM, Jin H, Marshall CB, Schafer JM, Sheng Q, et al. Acquisition of aneuploidy drives mutant p53-associated gain-of-function phenotypes. Nat Commun 2021;12:5184.
8. Wang Z, Burigotto M, Ghetti S, Vaillant F, Tan T, Capaldo BD, et al. Loss-of-Function but not gain-of-function properties of mutant TP53 are critical for the proliferation, survival, and metastasis of a broad range of cancer cells. Cancer Discov 2024;14:362–79.
9. Hoyos D, Zappasodi R, Schulze I, Sethna Z, de Andrade KC, Bajorin DF, et al. Fundamental immune-oncogenicity trade-offs define driver mutation fitness. Nature 2022;606:172–9.
10. Richardson CD, Ray GJ, DeWitt MA, Curie GL, Corn JE. Enhancing homology-directed genome editing by catalytically active and inactive CRISPR-Cas9 using asymmetric donor DNA. Nat Biotechnol 2016;34:339–44.
11. Salmon P, Trono D. Production and titration of lentiviral vectors. Curr Protoc Neurosci 2006;Chapter 12:Unit 12.10.
12. Jan M, Scarfò I, Larson RC, Walker A, Schmidts A, Guirguis AA, et al. Reversible ON- and OFF-switch chimeric antigen receptors controlled by lenalidomide. Sci Transl Med 2021;13:eabb6295.
13. Stewart-Ornstein J, Lahav G. Dynamics of CDKN1A in single cells defined by an endogenous fluorescent tagging toolkit. Cell Rep 2016;14:1800–11.
14. Banning C, Votteler J, Hoffmann D, Koppensteiner H, Warmer M, Reimer R, et al. A flow cytometry-based FRET assay to identify and analyse protein-protein interactions in living cells. PLoS One 2010;5:e9344.
15. Nicholls CD, McLure KG, Shields MA, Lee PW. Biogenesis of p53 involves cotranslational dimerization of monomers and posttranslational dimerization of dimers. Implications on the dominant negative effect. J Biol Chem 2002;277:12937–45.
16. Natan E, Hirschberg D, Morgner N, Robinson CV, Fersht AR. Ultraslow oligomerization equilibria of p53 and its implications. Proc Natl Acad Sci U S A 2009;106:14327–32.
17. Haupt Y, Maya R, Kazaz A, Oren M. Mdm2 promotes the rapid degradation of p53. Nature 1997;387:296–9.
18. Kubbutat MH, Jones SN, Vousden KH. Regulation of p53 stability by Mdm2. Nature 1997;387:299–303.
19. Köbel M, Piskorz AM, Lee S, Lui S, LePage C, Marass F, et al. Optimized p53 immunohistochemistry is an accurate predictor of TP53 mutation in ovarian carcinoma. J Pathol Clin Res 2016;2:247–58.
20. Fernandez-Pol S, Ma L, Ohgami RS, Arber DA. Immunohistochemistry for p53 is a useful tool to identify cases of acute myeloid leukemia with myelodysplasia-related changes that are TP53 mutated, have complex karyotype, and have poor prognosis. Mod Pathol 2017;30:382–92.
21. Sievers QL, Petzold G, Bunker RD, Renneville A, Słabicki M, Liddicoat BJ, et al. Defining the human C2H2 zinc finger degrome targeted by thalidomide analogs through CRBN. Science 2018;362:eaat0572.

22. Willis A, Jung EJ, Wakefield T, Chen X. Mutant p53 exerts a dominant negative effect by preventing wild-type p53 from binding to the promoter of its target genes. Oncogene 2004;23:2330–8.
23. Chan WM, Siu WY, Lau A, Poon RY. How many mutant p53 molecules are needed to inactivate a tetramer? Mol Cell Biol 2004;24:3536–51.
24. Varley JM, Thorncroft M, McGown G, Appleby J, Kelsey AM, Tricker KJ, et al. A detailed study of loss of heterozygosity on chromosome 17 in tumours from Li-Fraumeni patients carrying a mutation to the TP53 gene. Oncogene 1997; 14:865–71.
25. Joerger AC, Fersht AR. The p53 pathway: origins, inactivation in cancer, and emerging therapeutic approaches. Annu Rev Biochem 2016;85: 375–404.
26. Forget KJ, Tremblay G, Roucou X. p53 Aggregates penetrate cells and induce the co-aggregation of intracellular p53. PLoS One 2013;8:e69242.
27. Silva JL, Rangel LP, Costa DC, Cordeiro Y, De Moura Gallo CV. Expanding the prion concept to cancer biology: dominant-negative effect of aggregates of mutant p53 tumour suppressor. Biosci Rep 2013;33:e00054.
28. Silva JL, De Moura Gallo CV, Costa DC, Rangel LP. Prion-like aggregation of mutant p53 in cancer. Trends Biochem Sci 2014;39:260–7.
29. Yang H, Hu HY. Sequestration of cellular interacting partners by protein aggregates: implication in a loss-of-function pathology. FEBS J 2016;283:3705–17.
30. Yue X, Zhao Y, Xu Y, Zheng M, Feng Z, Hu W. Mutant p53 in cancer: accumulation, gain-of-function, and therapy. J Mol Biol 2017;429:1595–606.
31. Iyer SV, Parrales A, Begani P, Narkar A, Adhikari AS, Martinez LA, et al. Allele-specific silencing of mutant p53 attenuates dominant-negative and gain-of-function activities. Oncotarget 2016;7:5401–15.
32. Ubby I, Krueger C, Rosato R, Qian W, Chang J, Sabapathy K. Cancer therapeutic targeting using mutant-p53-specific siRNAs. Oncogene 2019;38:3415–27.